
Beyond DAGs: A Latent Partial Causal Model for Multimodal Learning

Yuhang Liu*

The University of Adelaide

Zhen Zhang

The University of Adelaide

Dong Gong

The University of New South Wales

Erdun Gao

The University of Adelaide

Biwei Huang

University of California San Diego

Mingming Gong

The University of Melbourne

Anton van den Hengel

The University of Adelaide

Kun Zhang

Carnegie Mellon University

Javen Qinfeng Shi

The University of Adelaide

Abstract

Directed acyclic graphs (DAGs) are fundamental graph structures in causal modeling, but identifying the desired DAG from observational data often requires strong assumptions that may not hold in real-world scenarios, especially for latent causal models and complex multimodal data. This raises the question of whether we can relax or bypass the DAG assumption while maintaining practical utility. In this work, we propose a novel latent partial causal model for multimodal data, featuring two latent coupled variables, connected by an undirected edge, to represent the transfer of knowledge across modalities. Under specific statistical assumptions, we establish an identifiability result, demonstrating that representations learned by multimodal contrastive learning correspond to the latent coupled variables up to a trivial transformation. This result deepens our understanding of why multimodal contrastive learning works, highlights its potential for disentanglement, and expands the utility of pre-trained models like CLIP. Synthetic experiments confirm the robustness of our findings, even when the assumptions are partially violated. Most importantly, experiments on a pre-trained CLIP model embodies disentangled representations, enabling few-shot learning and improving domain generalization across diverse real-world datasets. Together, these contributions push the boundaries of multimodal contrastive learning, both theoretically and, crucially, in practical applications.

1 Introduction

The adoption of a directed acyclic graph (DAG) as the underlying graph structure is a foundational assumption in most causal modeling methods [45, 55]. Identifying the DAG typically requires additional assumptions that enforce the asymmetry between nodes, allowing for the distinction of causes and effects [13]. In causal discovery within the observed space, these assumptions often include imposing constraints on the function class, such as linear non-Gaussian [53] or additive noise models [21, 46]. However, due to the complex and uncertain nature of real-world data, justifying these restrictive function classes is often impractical.

*yuhang.liu01@adelaide.edu.au

This challenge becomes even more pronounced in latent spaces, such as in causal representation learning (CRL) [51], where the relationships among observational data are assumed to arise from causal interactions between high-level latent causal variables. Most existing methods for identifying latent causal variables rely on the assumption that data resulting from interventions on all latent variables are available [36, 4, 5, 57, 1, 52, 37]. However, acquiring such interventional data can be difficult, and in many cases, it may be impossible in real-world scenarios.

This challenge is further amplified in multimodal settings, as the causal relationships across different modalities often involve intricate dependencies that may not conform to a single global DAG structure. This raises a fundamental question: can we develop a more general latent causal modeling framework for multimodal settings that relaxes or circumvents DAG structure assumption while maintaining practical utility in real-world scenarios?

We introduce a novel latent partial causal generative model in this work, to characterize the multimodal data generative process, as depicted in Figure 1. Unlike traditional DAG assumptions, our framework introduces latent coupled variables linked by an undirected edge to represent the transfer of knowledge across modalities, enabling flexible modeling of complex dependencies. Additionally, the model incorporates modality-specific latent variables to capture distinct information within each modality and employs dedicated mappings from the latent space to the observed space, facilitating data generation tailored to each modality.

Building on the proposed latent partial causal *generative model*, we examine its relationship with multimodal contrastive learning, a widely-adopted *inference model* [64, 47]. Through identifiability analysis, we establish a theoretical link between the generative and inference models, showing that the representations learned by multimodal contrastive learning correspond to the latent coupled variables in the generative model. This correspondence holds up to a trivial linear transformation in hypersphere space and a permutation transformation in convex bodies. These results provide a theoretical foundation for the success of multimodal contrastive learning.

Furthermore, our linear identifiability results in hypersphere space and permutation identifiability in convex bodies provide strong theoretical justification for the disentanglement capabilities of multimodal contrastive learning, under the assumption that each latent coupled variable is mutually independent. This offers a surprising insight into leveraging the disentanglement potential of CLIP-like models [47], trained by multimodal contrastive learning, to address tasks that rely on disentangled representations. For instance, this potential can be utilized to enable the learning of disentangled representations, enhance performance in few-shot learning and domain generalization.

In summary, our contributions are as follows:

- We propose a novel latent partial causal model for the generative process, specifically designed for multimodal data. Instead of relying on DAGs assumption, our model introduces latent coupled variables, connected by undirected edges, to effectively capture transferable knowledge across modalities.
- Our identifiability analysis demonstrates that the representations learned by multimodal contrastive learning align with latent coupled variables in the generative model. This insight highlights that the success of multimodal contrastive learning lies in its capacity to identify these latent variables within generative models.
- Furthermore, our identifiability results establish the theoretical basis for the component-wise disentanglement potential of multimodal contrastive learning. This pushes the boundaries of how pre-trained models, such as CLIP, can be leveraged. *To the best of our knowledge, this is the first work to provide guarantees for the component-wise disentanglement potential.*
- We validate our theoretical findings under ideal conditions and demonstrate their robustness even when assumptions are partially violated. Extensive experiments on pre-trained CLIP model across various tasks—such as few-shot learning, domain generalization, and disentangled representation learning—on over 16 real-world datasets substantiate the practical effectiveness of latent coupled models. *We emphasize that, unlike prior works on identifiability analysis for multimodal learning [8, 62, 14], which are limited to simulation experiments, this work empirically validates identifiability results using real datasets and models, thereby demonstrating the robustness and practical significance of our theoretical findings.*

In conclusion, the proposed latent partial causal model supports the success of multimodal contrastive learning and reveals its potential for disentanglement. Most importantly, experiments on pre-trained CLIP across various tasks using extensive real-world data demonstrate the practical utility of our theoretical results. Collectively, these findings relax the conventional reliance on DAG assumptions in multimodal contrastive learning, while maintaining practical utility in real-world scenarios.

2 Generative Model: The Latent Partial Causal Model

In this section, we introduce a novel latent partial causal model designed to represent the generative process of multimodal data. Unlike traditional DAG assumptions, our model incorporates an undirected edge between two latent variables, enabling the capture of transferable knowledge across modalities, as depicted in Figure 1. This non-DAG structure offers substantial flexibility, allowing the representation of multiple DAG assumptions as special cases, as illustrated in Figure 2. By doing so, our model facilitates the extraction of transferable latent knowledge that underpins the fundamental principles behind various DAG assumptions, thereby enabling a more flexible and generalized approach to multimodal causal modeling.

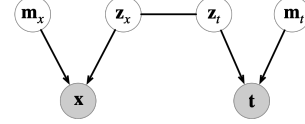


Figure 1: The proposed latent partial causal model. z_x and z_t are latent coupled variables, and m_x , m_t are modality-specific.

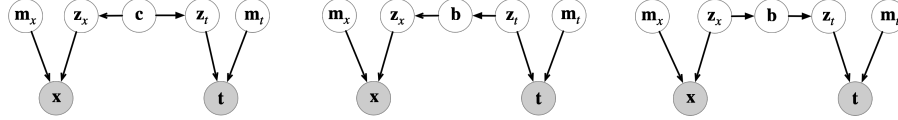


Figure 2: Illustrative DAGs behind the proposed model: Left: A latent confounder influences both z_x and z_t . Middle: z_t influences z_x through an intermediate mediator b , serving as a bottleneck for transferable knowledge. Right: A symmetric inverse relationship where z_x influences z_t via b .

The Proposed Latent Partial Causal Models Figure 1 illustrates the proposed latent partial causal model, designed to represent the generative process for multimodal data. The latent space is partitioned into two components, each corresponding to a specific modality, such as image and text. To capture unique characteristics within each domain, the model incorporates modality-specific latent variables, m_x and m_t tailored. For instance, m_x may represent domain-specific aspects such as background noise or visual artifacts, while m_t could encode linguistic features such as sentence structure or grammatical patterns. Further, the observations are generated through distinct processes that link the latent variables to the observed data. Specifically, images (x) are generated by the function $g_x(m_x, z_x)$, while text (t) is produced by $g_t(m_t, z_t)$.

In addition, to capture transferable knowledge between these modalities, the model introduces an undirected edge between the latent coupled variables, z_x and z_t . The rationale behind this modeling approach is grounded in the intricate dependencies between modalities. For instance, the adage “a picture is worth a thousand words” highlights the richness and detail of visual data, as supported by [15, 23]. However, this perspective is not universally applicable, as [49] argues that textual information can often convey more precise meanings. Similarly, [11] reinforces the complementary nature of text, asserting that “a sentence is worth a thousand pixels” in its ability to succinctly express complex ideas.

Beyond the rationale outlined above for introducing coupled variables and an undirected edge between them, two key factors justify this design: 1) *Modality Gap*: In multimodal models like CLIP [35], different data modalities are often embedded at a distance in the shared representation space. This suggests that using two coupled variables to represent transferable knowledge across modalities may be appropriate. 2) *The diversity of real-world multimodal data*: Real-world multimodal data often entails complex dependencies that a single global structure may fail to capture. More importantly, these dependencies could even be represented by conflicting directed acyclic graphs (DAGs). Figure 2 illustrates such potential DAGs, offering insights into the diverse underlying causal structures.

In the left DAG of Figure 2, the latent confounder c represents a shared source of variation that influences both z_x and z_t . This confounder captures a common underlying context or concept connecting the two modalities. For example, if the image and text are related to the topic “sports,” c

could encapsulate this shared theme, influencing the generation of both the visual and textual data. The middle DAG depicts a structure where \mathbf{b} , representing transferable knowledge. Specifically, \mathbf{b} serves as the bridge, deriving information from the text latent variable \mathbf{z}_t and informing the image latent space \mathbf{z}_x . This scenario aligns with tasks where text serves as a guiding input for image generation, e.g., text-to-image generalization. A classical example is the MNIST dataset. In contrast, the DAG on the right represents an image-guided text generation process, e.g., image captioning. Here, the high-level latent information in the image influences the high-level latent variable in the generated caption. A classical example is the CelebA-Dialog dataset [31].

3 A First Look: The Recovery Potential of Multimodal Contrastive Learning

Given the proposed latent coupled generative model, as depicted by Figure 1, our final goal is to analyze how multimodal contrastive learning framework can recover the true latent coupled variables, up to an sample transformation. Before this, we first provide an intuitive motivation to explain why we believe multimodal contrastive learning can achieve this.

Multimodal contrastive learning leverages a loss function designed to maximize similarity between embeddings of real paired data while minimizing similarity for incorrect pairs. The loss function is defined as [64, 47]:

$$\mathcal{L} = -\frac{1}{N} \sum_{i=1}^N \log \frac{e^{-d(\mathbf{f}_x(\mathbf{x}_i), \mathbf{f}_t(\mathbf{t}_i))/\tau}}{\sum_{j=1}^N e^{-d(\mathbf{f}_x(\mathbf{x}_i), \mathbf{f}_t(\mathbf{t}_j))/\tau}} - \frac{1}{N} \sum_{i=1}^N \log \frac{e^{-d(\mathbf{f}_x(\mathbf{x}_i), \mathbf{f}_t(\mathbf{t}_i))/\tau}}{\sum_{j=1}^N e^{-d(\mathbf{f}_x(\mathbf{x}_j), \mathbf{f}_t(\mathbf{t}_i))/\tau}}, \quad (1)$$

where d denotes a distance metric, e.g., cosine similarity on hypersphere or L1 norm on convex bodies, τ is a learnable temperature parameter, N denotes the sample size, which means that we have N positive pairs and $N^2 - N$ negative pairs, \mathbf{f}_x denote the encoder on one modality \mathbf{x} , i.e., image, similarly, \mathbf{f}_t denote the encoder on another \mathbf{t} , i.e., text.

To understand the multimodal contrastive loss further, we investigate its asymptotics:

Theorem 3.1 (Asymptotics of \mathcal{L}). *For fixed $\tau > 0$, as the sample size $N \rightarrow \infty$, the (normalized) multimodal contrastive loss converges to*

$$\begin{aligned} \lim_{N \rightarrow \infty} \mathcal{L} - 2 \log N = & 2 \mathbb{E}_{(\mathbf{x}, \mathbf{t}) \sim p(\mathbf{x}, \mathbf{t})} [d(\mathbf{f}_x(\mathbf{x}), \mathbf{f}_t(\mathbf{t}))/\tau] + \mathbb{E}_{\mathbf{x} \sim p(\mathbf{x})} \left[\log \mathbb{E}_{\mathbf{t} \sim p(\mathbf{t})} [e^{-d(\mathbf{f}_x(\mathbf{x}), \mathbf{f}_t(\mathbf{t}))/\tau}] \right] \\ & + \mathbb{E}_{\mathbf{t} \sim p(\mathbf{t})} \left[\log \mathbb{E}_{\mathbf{x} \sim p(\mathbf{x})} [e^{-d(\mathbf{f}_x(\mathbf{x}), \mathbf{f}_t(\mathbf{t}))/\tau}] \right]. \end{aligned} \quad (2)$$

This result extends Theorem 1 from [60] to the multimodal context. Proof is provided in Appendix B.

Insights into Latent Variable Recovery The loss function in Eq. (2) connects directly to two fundamental principles in latent variable recovery: Prior Matching and Information Preservation. These principles are crucial for methods like nonlinear independent component analysis (ICA) [28], which recover latent independent variables from observed data.

- *Prior Matching*: This constrains the solution space using prior knowledge, addressing the non-uniqueness problem that often arises in latent variable recovery.
- *Information Preservation*: This ensures that the solution space fully captures the complexity of the latent variables derived from the observed data.

Prior Matching The first term in Eq. (2) promotes alignment between representations of real data pairs across modalities, enforcing that one modality (i.e., text) acts as a prior signal for the other (i.e., image). Minimizing this term drives cross-modal alignment and incorporates prior knowledge, which is key for recovering latent variables.

Information Preservation The last two terms in Eq. (2) are closely related to ensuring that the learned representations capture the full complexity of the latent variables. These terms can be approximated by optimizing the following expression (proof in Appendix C):

$$-H(p(\mathbf{f}_x(\mathbf{x})), p(\mathbf{f}_t(\mathbf{t}))) - H(p(\mathbf{f}_t(\mathbf{t})), p(\mathbf{f}_x(\mathbf{x}))), \quad (3)$$

where $H(\cdot, \cdot)$ denotes cross-entropy. The objective function in Eq. (2) is symmetric between \mathbf{x} and \mathbf{t} . Intuitively, if $p(\mathbf{f}_x(\mathbf{x}))$ and $p(\mathbf{f}_t(\mathbf{t}))$ are not equal, the solution deviates, increasing the objective value and introducing asymmetry in the last two terms. For the optimal solution, the two distributions must align. When $p(\mathbf{f}_x(\mathbf{x})) = p(\mathbf{f}_t(\mathbf{t}))$, the cross-entropy in Eq. (3) reduces to entropy, and if \mathbf{f}_x and \mathbf{f}_t transform \mathbf{x} and \mathbf{t} into uniformly distributed random variables, Eq. (3) reaches its optimal value. This highlights the importance of finding transformations \mathbf{f}_x and \mathbf{f}_t that preserve information by fully capturing the latent variable structure.

A Novel Unified Perspective on Contrastive Loss Previous research has primarily focused on contrastive loss in the context of single modalities, emphasizing two main perspectives: 1) alignment-uniformity [60], which is closely related to prior matching, and 2) information preservation [43]. However, these perspectives have largely been treated separately. In this work, we offer a novel insight by combining these two perspectives within the multimodal context for latent variable recovery. This insight motivates our belief that multimodal contrastive representation learning holds significant potential for recovering latent variables.

4 From Potential to Principles: Identifiability Guarantee

Given the initiative analysis in Section 3, which highlights the potential of multimodal contrastive learning for recovering latent variables, we now move forward to rigorous identifiability analysis, which provide theoretical guarantees that multimodal contrastive learning can indeed recover the true latent variables, by parameterizing the proposed latent partial causal model. We examine two distinct types of parameterization in latent spaces, hyperspheres and convex bodies, under specific assumptions, respectively.

4.1 Identifiability Analysis on Hypersphere

On hypersphere, we parameterize the proposed latent partial causal generative models as following:

$$p(\mathbf{z}_x) = |\mathcal{Z}|^{-1}, \quad p(\mathbf{z}_t|\mathbf{z}_x) = C_p^{-1} e^{(k\mathbf{z}_t^T \mathbf{z}_x)}, \quad \mathbf{x} = \mathbf{g}_x(\mathbf{z}_x, \mathbf{m}_x), \quad \mathbf{t} = \mathbf{g}_t(\mathbf{z}_t, \mathbf{m}_t), \quad (4)$$

where \mathcal{Z} denotes the space of latent factors \mathbf{z}_x and \mathbf{z}_t . We assume that \mathcal{Z} is the unit hypersphere \mathbb{S}^{M-1} , aligning with the commonly used normalization in constrastive loss. We do not enforce any further assumptions for \mathbf{m}_x and \mathbf{m}_t . For \mathbf{g}_x and \mathbf{g}_t , we assume them to be nonlinear, and invertible (*i.e.*, injective) mapping, ensuring the information in latent space can be recovered. In addition, we assume that $p(\mathbf{z}_x)$ follows a uniform distribution, and $p(\mathbf{z}_t|\mathbf{z}_x)$ follows a von Mises-Fisher (vMF) distribution, considering the constraint of unit hypersphere. Given these assumptions, we first establish that the minimization of the symmetric cross-entropy Eq. (2)) converges to a symmetric cross entropy, as follows:

Theorem 4.1. (*\mathcal{L} converges to the symmetric cross-entropy*) Under the assumptions defined in Eqs. (4) for the proposed latent partial causal model, the necessary condition $\mathbf{f}_x \circ \mathbf{g}_x = \mathbf{f}_t \circ \mathbf{g}_t$, denoted as \mathbf{h} , for the optimal normalized multimodal contrastiveloss given by Eq. (2) leads to the following reduction of the loss itself:

$$\lim_{N \rightarrow \infty} \mathcal{L} - 2 \log N + 2 \log |\mathcal{Z}| = \mathbb{E}_{\mathbf{z}_x \sim p(\mathbf{z}_x)} [H(p(\mathbf{z}_t|\mathbf{z}_x), q_{\mathbf{h}}(\mathbf{z}_t|\mathbf{z}_x))] + \mathbb{E}_{\mathbf{z}_t \sim p(\mathbf{z}_t)} [H(p(\mathbf{z}_x|\mathbf{z}_t), q_{\mathbf{h}}(\mathbf{z}_x|\mathbf{z}_t))], \quad (5)$$

where H is the cross entropy, the conditional distributions $q_{\mathbf{h}}(\mathbf{z}_t|\mathbf{z}_x)$ and $q(\mathbf{z}_x|\mathbf{z}_t)$ are parameterized by the following:

$$q_{\mathbf{h}}(\mathbf{z}_x|\mathbf{z}_t) = C_q(\mathbf{z}_t)^{-1} e^{(\mathbf{h}(\mathbf{z}_x)^T \mathbf{h}(\mathbf{z}_t)/\tau)} q_{\mathbf{h}}(\mathbf{z}_t|\mathbf{z}_x) = C_q(\mathbf{z}_x)^{-1} e^{(\mathbf{h}(\mathbf{z}_t)^T \mathbf{h}(\mathbf{z}_x)/\tau)}, \quad (6)$$

with

$$C_q(\mathbf{z}_t) = \int e^{(\mathbf{h}(\mathbf{z}_x)^T \mathbf{h}(\mathbf{z}_t)/\tau)} d\mathbf{z}_x, C_q(\mathbf{z}_x) = \int e^{(\mathbf{h}(\mathbf{z}_x)^T \mathbf{h}(\mathbf{z}_t)/\tau)} d\mathbf{z}_t.$$

Refer to Appendix D.1 for proof. This is a generalization of Theorem 1 in [67].

Bridge Between Modalities By addressing key asymmetries arising from modality differences, such as modality-specific variables \mathbf{m}_x and \mathbf{m}_t , along with distinct generative processes \mathbf{g}_x and \mathbf{g}_t , we derive the result in Theorem 4.1. This result is pivotal as it establishes a critical connection between multimodal contrastive learning and traditional single-modal contrastive learning. In particular, Theorem 4.1 enables the transfer of insights and results from single-modal settings to the multimodal context. As a result, we present the following corollary:

Corollary 4.2. *By leveraging Theorem 4.1, the minimization of Eq. (5) identifies the latent variables \mathbf{z}_x (and symmetrically, \mathbf{z}_t) up to a linear transformation. Specifically, the representations $\mathbf{f}_x(\mathbf{x})$, learned by the minimization of Eq. (5), are linearly related to the underlying latent variables \mathbf{z}_x in the proposed latent partial causal model, as follows: $\mathbf{f}_x(\mathbf{x}) = \mathbf{A}\mathbf{z}_x + \mathbf{c}$, where \mathbf{A} is an orthogonal matrix and \mathbf{c} is a constant vector.*

For further details, see Appendix D.2.

Success of Multimodal Contrastive Learning Corollary 4.2 shows that minimizing Eq. (5) (or equivalently, the multimodal contrastive loss in Eq. (1)) identifies the latent variables \mathbf{z}_x (and symmetrically, \mathbf{z}_t) up to a linear transformation. This means that the representations $\mathbf{f}_x(\mathbf{x})$, learned through multimodal contrastive learning, are directly related to the latent variables \mathbf{z}_x via a linear transformation, i.e., $\mathbf{f}_x(\mathbf{x}) = \mathbf{A}\mathbf{z}_x + \mathbf{c}$. A similar result holds for \mathbf{z}_t . This finding highlights the effectiveness of multimodal contrastive learning, suggesting that its success in practical applications stems from its ability to recover latent coupled variables. This recovery preserves essential, transferable knowledge across modalities, enabling the learned representations to capture high-level transferable information while discarding model-specific details. Such properties are key to the robustness and transferability of multimodal contrastive learning representations.

4.2 Identifiability Analysis on Convex Bodies

We now extend the previous identifiability result to convex bodies, e.g., the hyperrectangle $[a_1, b_1] \times \dots \times [a_M, b_M]$. On convex bodies, we parameterize the proposed generative models by the following:

$$p(\mathbf{z}_x) = |\mathcal{Z}_c|^{-1}, \quad p(\mathbf{z}_t|\mathbf{z}_x) = C_p(\mathbf{z}_x)^{-1} e^{-\delta(\mathbf{z}_t, \mathbf{z}_x)/\lambda}, \quad \mathbf{x} = \mathbf{g}_x(\mathbf{z}_x, \mathbf{m}_x), \quad \mathbf{t} = \mathbf{g}_t(\mathbf{z}_t, \mathbf{m}_t), \quad (7)$$

where δ is a distance metric induced by a norm. We consider a convex body in \mathbb{R}^M , denoted as \mathcal{Z}_c , where we assume that $p(\mathbf{z}_x)$ follows a uniform distribution, and the conditional distribution $p(\mathbf{z}_t|\mathbf{z}_x)$ follows an exponential distribution. Again, we do not enforce any further assumptions for \mathbf{m}_x and \mathbf{m}_t . For \mathbf{g}_x and \mathbf{g}_t , we assume them to be nonlinear and invertible mapping, ensuring information in latent space can be recovered. Given these assumptions, we have the following result:

Theorem 4.3. (\mathcal{L} converges to the symmetric cross-entropy) *Under the assumptions defined in Eq. (7) for the proposed latent partial causal model, the necessary condition $\mathbf{f}_x \circ \mathbf{g}_x = \mathbf{f}_t \circ \mathbf{g}_t$, denoted as \mathbf{h} , for the optimal normalized multimodal contrastive loss given by Eq. (2) leads to the following reduction of the loss itself:*

$$\lim_{N \rightarrow \infty} \mathcal{L} - 2 \log N + 2 \log |\mathcal{Z}_c| = \mathbb{E}_{\mathbf{z}_x \sim p(\mathbf{z}_x)} [H(p(\mathbf{z}_t|\mathbf{z}_x), q_{\mathbf{h}}(\mathbf{z}_t|\mathbf{z}_x))] + \mathbb{E}_{\mathbf{z}_t \sim p(\mathbf{z}_t)} [H(p(\mathbf{z}_x|\mathbf{z}_t), q_{\mathbf{h}}(\mathbf{z}_x|\mathbf{z}_t))], \quad (8)$$

where H is the cross entropy, the conditional distributions $q_{\mathbf{h}}(\mathbf{z}_t|\mathbf{z}_x)$ and $q(\mathbf{z}_x|\mathbf{z}_t)$ are parameterized by the following:

$$q_{\mathbf{h}}(\mathbf{z}_x|\mathbf{z}_t) = C_q(\mathbf{z}_t) e^{-\delta(\mathbf{h}(\mathbf{z}_x), \mathbf{h}(\mathbf{z}_t))/\tau}, \quad q_{\mathbf{h}}(\mathbf{z}_t|\mathbf{z}_x) = C_q(\mathbf{z}_x) e^{-\delta(\mathbf{h}(\mathbf{z}_x), \mathbf{h}(\mathbf{z}_t))/\tau}, \quad (9)$$

with

$$C_q(\mathbf{z}_t) = \int e^{-\delta(\mathbf{h}(\mathbf{z}_x), \mathbf{h}(\mathbf{z}_t))/\tau} d\mathbf{z}_x, \quad C_q(\mathbf{z}_x) = \int e^{-\delta(\mathbf{h}(\mathbf{z}_x), \mathbf{h}(\mathbf{z}_t))/\tau} d\mathbf{z}_t.$$

Bridge Between Modalities In convex bodies, Theorem 4.3, introduced for the first time in this work, plays a key role in bridging multimodal contrastive learning with traditional contrastive learning by addressing the asymmetric challenges arising from modality differences. Building on this theorem, we can seamlessly extend the findings of Theorem 5 from the single-modal context [67] to the multimodal setting, as follows:

Corollary 4.4. *By leveraging Theorem 4.3, the minimization of Eq. (8) in theorem 4.3 identifies the latent variables \mathbf{z}_x (symmetrically, \mathbf{z}_t) up to a permutation transformation, i.e., the representations $\mathbf{f}_x(\mathbf{x})$, learned by the minimization of Eq. (8), is related to the underlying \mathbf{z}_x in the proposed partial causal model as follows: $\mathbf{f}_x(\mathbf{x}) = \mathbf{P}\mathbf{z}_x + \mathbf{c}$, where \mathbf{P} is a permutation matrix with scaling, \mathbf{c} is a constant vector.*

For completeness, see details in Appendix E.2.

Success of Multimodal Contrastive Learning Corollary 4.2 Similar to Corollary 4.2 on hyperspheres, Corollary 4.4 establishes that, on convex bodies, the representations $\mathbf{f}_x(\mathbf{x})$ learned by multimodal contrastive learning are related to the true latent variables \mathbf{z}_x as $\mathbf{f}_x(\mathbf{x}) = \mathbf{P}\mathbf{z}_x + \mathbf{c}$. This provides a theoretical foundation for the success of multimodal contrastive learning on convex bodies.

5 From Principles to Practice: Disentanglement Ability of CLIP-like Models

In theory, both Corollaries 4.2 and 4.4 suggest a disentanglement potential of CLIP-like models trained by multimodal contrastive learning, under the assumption that the variables in \mathbf{z}_x (and symmetrically, \mathbf{z}_t) are mutually independent. we explore how these theoretical insights can be translated into practical guidance for the effective use of CLIP-like models.

Corollary 4.2 shows that the representations $\mathbf{f}_x(\mathbf{x})$ learned by multimodal contrastive learning are linearly related to the true latent variables \mathbf{z}_x via an orthogonal transformation, i.e., $\mathbf{f}_x(\mathbf{x}) = \mathbf{A}\mathbf{z}_x + \mathbf{c}$. This result holds under two key conditions: (1) the true latent variables are sampled from a hyperspherical latent space, and (2) the inference model, e.g., CLIP-like models, is trained in a hyperspherical inference space. Notably, CLIP-like models naturally satisfy condition (2), as they typically employ L2 normalization, constraining representations to the unit sphere. Therefore, under condition (1) holds, the representations from CLIP-like models can be passed through linear unmixing method (e.g., FastICA [24]) to resolve the mixing matrix \mathbf{A} , resulting in disentangled representations. It is worth to note that the geometry of the hypersphere, specifically the unit $M - 1$ -dimensional hypersphere, places an upper bound on the number of independent variables, i.e., $M - 1$ at most.

Unlike Corollary 4.2, Corollary 4.4 shows that the learned representations $\mathbf{f}_x(\mathbf{x})$ from multimodal contrastive learning are already disentangled, i.e., $\mathbf{f}_x(\mathbf{x}) = \mathbf{P}\mathbf{z}_x + \mathbf{c}$. This result mainly requires two conditions: (1) the true latent variables \mathbf{z}_x are sampled from a convex body latent space, and (2) the inference space of the model is also constrained to a convex body. However, CLIP-like models typically violate the second condition, as they operate in a hyperspherical inference space due to L2 normalization, even though we assume that the first condition may hold. Nevertheless, the insight from Corollary 4.4 remains useful with appropriate adjustments. In particular, the Corollary relies on the existence of an isometric mapping from the latent space to the representation space (see Eq. 48 in the Appendix). Although a global isometry from a convex body to a hypersphere is not feasible, it is reasonable to assume a local isometry between the convex body and small regions of the hypersphere. Based on this, we propose first applying Principal Component Analysis (PCA) to the representations $\mathbf{f}_x(\mathbf{x})$. Then, FastICA can be used to account for the orthogonal transformation introduced by PCA, enabling the extraction of the final disentangled representations. This PCA+ICA pipeline thus enables effective use of CLIP-like models under the result of Corollary 4.4.

By leveraging the disentanglement capabilities of CLIP-like models, we can improve performance on tasks that benefit from disentangled representations, such as few-shot learning and domain generalization. We hope this motivates further exploration of the disentanglement potential inherent in CLIP-like models across a broad range of downstream applications.

6 Synthetic Experiments and Real-World Evaluation with Pretrained CLIP

Synthetic Experiments In our initial experiments, we use synthetic data to validate our main identifiability results on hyperspheres and convex bodies, while also empirically assessing their robustness under significant violations of assumptions. We first sample $p(\mathbf{z}_x)$ according to the distributions listed in Table 1. Additionally, we generate paired samples from the conditional distribution $p(\mathbf{z}_t|\mathbf{z}_x)$ following the distributions specified in the same table. Beyond hyperspheres, our experiments also consider bounded and unbounded spaces. Each experiment is repeated three times for every setting. For more details regarding experiments, refer to Appendix K.

Table 1: Assessing identifiability up to linear (a) and permutation (b) transformations under varying assumptions. The first row in (a) and the first two rows in (b) represent settings that align with our assumptions in Corollary 4.2 and Corollary 4.4, while the others show results for violated assumptions. S: Space, Sp: Sphere, U: Uniform, v: vMF ($k = 1$), L: Laplace ($\lambda = 0.05$), N: Normal ($\delta = 0.05$), B: Box, Un: Unbounded, G: GenNorm($\beta = 3$).

Generative process			Model		R2
S	$p(\mathbf{z}_x)$	$p(\mathbf{z}_x \mathbf{z}_t)$	S	$q(\mathbf{z}_x \mathbf{z}_t)$	
Sp	U	v	Sp	v	99.5 ± 0.1
Sp	U	L	Sp	v	99.4 ± 0.2
Sp	U	N	Sp	v	98.7 ± 0.3
B	U	N	Un	N	90.5 ± 0.2
B	U	L	Un	N	92.2 ± 0.3
B	U	L	Un	G	99.1 ± 0.4
B	U	N	Un	G	91.2 ± 0.3
Sp	N ($\delta = 1$)	L	Sp	v	96.3 ± 0.3
Sp	N ($\delta = 1$)	N	Sp	v	95.9 ± 0.2
Un	L ($\lambda = 1$)	N	Un	N	88.5 ± 0.3
Un	N ($\delta = 1$)	N	Un	N	89.2 ± 0.2

Table 2: Assessing identifiability up to linear.

Generative process			Model		MCC
S	$p(\mathbf{z}_x)$	$p(\mathbf{z}_x \mathbf{z}_t)$	S	$q(\mathbf{z}_x \mathbf{z}_t)$	
B	U	L	B	L	99.1 ± 0.1
B	U	G	B	G	97.2 ± 0.3
B	U	N	B	N	98.6 ± 0.2
B	U	L	B	N	99.1 ± 0.1
B	U	G	B	L	98.4 ± 0.1
B	U	L	Un	L	95.6 ± 0.2
B	U	G	Un	G	96.4 ± 0.2

Table 3: Assessing identifiability up to permutation.

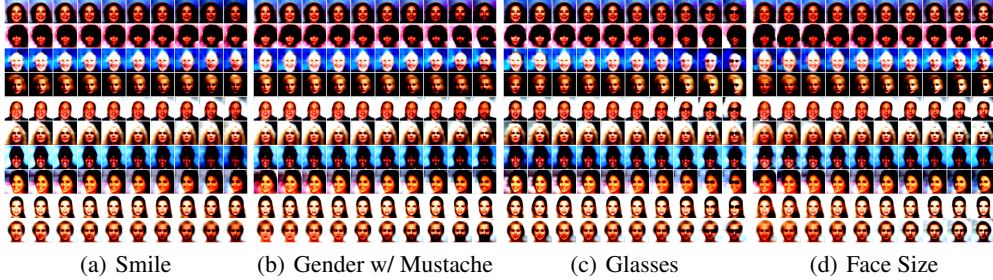


Figure 3: Disentangled Representations learned by combining pre-trained CLIP and FastICA. The results are aligned with our disentanglement findings.

To evaluate linear identifiability result in Corollary 4.2, we fit a linear regression model between the ground-truth \mathbf{z}_x and representations $\mathbf{f}_x(\mathbf{x})$ learned by multimodal contrastive learning and report the coefficient of determination (R^2). Further, to evaluate permutation identifiability result in Corollary 4.4, we employ the mean correlation coefficient (MCC) between the ground-truth \mathbf{z}_x and representations $\mathbf{f}_x(\mathbf{x})$ learned by multimodal contrastive learning. The first row in Table 1 (a) and the first two rows in Table 1 (b), corresponding to the setting where the assumptions are satisfied, verify the identifiability results on hypersphere and convex bodies, respectively. Our empirical investigations have yielded a critical insight: discrepancies in the assumptions concerning marginal and conditional distributions, as well as the nature of the spaces (hypersphere and convex body), do not significantly impact performance. This robustness is demonstrated by the results detailed in Table 1 (a) for the hypersphere space and Table 1 (b) for convex bodies. This observation is similar to reports from studies conducted in the context of single-model context [67]. This observation might be attributed to the fact that the loss function described in Eq. (2) predominantly relies on the computation of expectations, inherently allowing for a wide range of approximations. If we can approximate the expectation calculations consistently across various distributions and spaces, it might be reasonable that the identifiability results remain well within acceptable bounds.

Real-World Evaluation with Pretrained CLIP In the context of real data, the true latent coupled variables are unknown. Therefore, we evaluate our theoretical findings from the perspective of disentanglement as discussed in Section 5. *Again, we emphasize that, in contrast to previous studies on identifiability for multimodal contrastive learning [8, 62, 14], which rely on simulation experiments, this work validates identifiability through empirical analysis on real-world datasets and pre-trained CLIP model. This underscores the practicality of our theoretical contributions.*

Disentangled representations for CelebA data According to Section 5, we first extract representations from the pre-trained CLIP model and then apply FastICA to these representations to achieve final representations for CelebA data [38]. We expect these final representations to exhibit clear signs of disentanglement. To validate this, we proceed to train a decoder that reconstructs observational data using these extracted representations. Figure 3 illustrates the effectiveness of our method through latent space traversals. Specifically, it visualizes changes in reconstructions as we traverse one dimension of the latent space at a time, showcasing 4 out of 16 attributes uncovered by our approach. Additional results are available in Appendix H. This achievement not only validates our identifiability results, but also offers a new research line, i.e., learning disentangled representations by CLIP, or exploring how this disentanglement potential relate to the manipulation of pre-trained vision models, such as diffusion models.

Few-shot learning and domain generalization The goal of disentangled representations is to learn representations that transfer easily and robustly to downstream tasks, making them well-suited for few-shot learning and resilient to distribution shifts [12]. We thus focus on few-shot learning and domain generalization tasks to further evaluate our disentanglement findings. We extract representations from a limited set of labeled samples using a pre-trained CLIP model, combined with FastICA to align with the hypersphere, and with PCA followed by FastICA to align with convex body. These representations are then used to train a linear classifier. We evaluate the methods on ImageNet [9] for few-shot learning and test robustness on ImageNet-V2 [48], ImageNet-Sketch [59], ImageNet-R [19], and ImageNet-A [20]. Table 4 presents the performance metrics of the proposed methods in few-shot learning (as shown in the ‘SOURCE’ column) and domain generalization (indicated in the ‘TARGET’ columns). Analyzing the data in the SOURCE column reveals that the proposed methods outperform the baseline approach, which trains a linear classifier using representations directly obtained from pre-trained CLIP (i.e., the Linear Probe). This superior performance validates our disentanglement findings. Additionally, observations from the TARGET column further reinforce the benefits of disentanglement. Refer to Appendix I for more results.

Leveraging the Disentanglement Potential of CLIP-like Models for Few-Shot Learning In the final experiments, we demonstrate how the disentanglement potential pushes the boundaries of leveraging pre-trained models, e.g., CLIP. Recent progress shows that pre-trained CLIP’s adaptability can be significantly improved with just a few labeled training samples. The key to leveraging pre-trained CLIP for few-shot learning is effectively utilizing its extracted representations from limited labeled data, as Tip-Adapter and Tip-Adapter-F methods proposed in the work [63]. As we claim, leveraging disentangled potential of pre-trained CLIP can enhance performance on tasks that rely on disentangled representations, including few-shot learning. Therefore, rather than using CLIP’s raw representations, we apply FastICA to extract disentangled representations for few-shot tasks. This can be implemented in a plug-and-play way. As shown in Figure 5, incorpo-

Figure 4: Quantitative results for 2-shot learning and domain generalization by different methods. ①: Linear Probe, ②: ① with FastICA, and ③: ① with PCA and FastICA.

ENCODERS	METHODS	SOURCE		TARGET (ImageNet-)				
		ImageNet	V2	Sketch	R	A	Avg.	
RN50	①	31.95	26.48	8.41	20.74	7.44	15.77	
	②	34.06	28.74	8.37	21.72	10.15	17.25	
	③	34.12	28.68	11.55	25.57	10.15	18.99	
RN101	①	37.64	31.45	13.71	31.09	11.85	20.03	
	②	39.58	33.15	13.49	30.29	14.77	22.93	
	③	39.86	33.58	17.93	35.48	14.20	25.29	
ViT32	①	38.23	32.00	16.17	33.67	12.88	23.68	
	②	40.21	33.97	16.54	34.79	15.72	25.26	
	③	39.34	33.44	19.02	36.98	14.69	26.03	
ViT16	①	44.97	38.11	22.06	43.86	25.99	32.51	
	②	45.52	39.38	22.55	45.33	30.47	34.43	
	③	46.57	40.66	26.67	49.69	31.48	37.13	

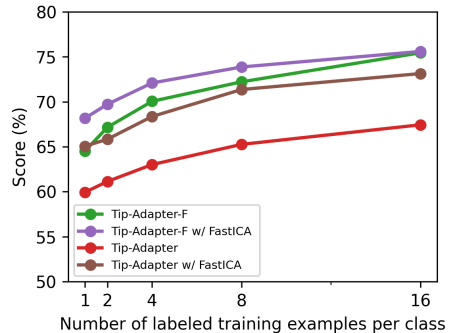


Figure 5: Comparison of accuracy (%) achieved by different few-shot CLIP adaptation methods across 11 datasets.

rating FastICA in the methods in [63], termed Tip-Adapter with FastICA and Tip-Adapter-F with FastICA, results in better performance, across 11 datasets, including ImageNet [9], Caltech101 [10], FGVC Aircraft [40], UCF101 [54], EuroSAT [18], Flowers102 [42], StanfordCars [34], DTD [7], Food101 [3], OxfordPets [44], and, SUN397 [61]. See Appendix J for more details.

7 Conclusion

In this work, we propose a novel latent partial causal model for multimodal data that moves beyond the traditional DAG structure, using latent coupled variables connected by undirected edges to capture transferable knowledge across modalities. We establish a theoretical link between this generative model and multimodal contrastive learning, showing that the representations learned by multimodal contrastive learning correspond to latent variables in the generative model, with linear and permutation transformations in hypersphere and convex body spaces, respectively. Our results provide the first theoretical guarantees for the disentanglement capabilities of multimodal contrastive learning, with applications in tasks like few-shot learning and domain generalization. Unlike prior simulation-based studies, our work demonstrates the real-world utility of multimodal contrastive learning and offers insights into leveraging pre-trained models like CLIP for disentangled representations. Our model challenges conventional DAG assumptions and provides a flexible, practical framework that enhances the effectiveness of multimodal contrastive learning.

References

- [1] K. Ahuja, D. Mahajan, Y. Wang, and Y. Bengio. Interventional causal representation learning. In *International Conference on Machine Learning*, pages 372–407. PMLR, 2023.
- [2] Y. Ban and Y. Dong. Pre-trained adversarial perturbations. *Advances in Neural Information Processing Systems*, 35:1196–1209, 2022.
- [3] L. Bossard, M. Guillaumin, and L. Van Gool. Food-101—mining discriminative components with random forests. In *Computer Vision—ECCV 2014: 13th European Conference, Zurich, Switzerland, September 6–12, 2014, Proceedings, Part VI 13*, pages 446–461. Springer, 2014.
- [4] J. Brehmer, P. De Haan, P. Lippe, and T. Cohen. Weakly supervised causal representation learning. *arXiv preprint arXiv:2203.16437*, 2022.
- [5] S. Buchholz, G. Rajendran, E. Rosenfeld, B. Aragam, B. Schölkopf, and P. Ravikumar. Learning linear causal representations from interventions under general nonlinear mixing. *arXiv preprint arXiv:2306.02235*, 2023.
- [6] R. T. Chen, X. Li, R. B. Grosse, and D. K. Duvenaud. Isolating sources of disentanglement in variational autoencoders. *Advances in neural information processing systems*, 31, 2018.
- [7] M. Cimpoi, S. Maji, I. Kokkinos, S. Mohamed, and A. Vedaldi. Describing textures in the wild. In *Proceedings of the IEEE conference on computer vision and pattern recognition*, pages 3606–3613, 2014.
- [8] I. Daunhawer, A. Bizeul, E. Palumbo, A. Marx, and J. E. Vogt. Identifiability results for multimodal contrastive learning. *arXiv preprint arXiv:2303.09166*, 2023.
- [9] J. Deng, W. Dong, R. Socher, L.-J. Li, K. Li, and L. Fei-Fei. Imagenet: A large-scale hierarchical image database. In *2009 IEEE conference on computer vision and pattern recognition*, pages 248–255. Ieee, 2009.
- [10] L. Fei-Fei, R. Fergus, and P. Perona. Learning generative visual models from few training examples: An incremental bayesian approach tested on 101 object categories. In *2004 conference on computer vision and pattern recognition workshop*, pages 178–178. IEEE, 2004.
- [11] S. Fidler, A. Sharma, and R. Urtasun. A sentence is worth a thousand pixels. In *Proceedings of the IEEE conference on Computer Vision and Pattern Recognition*, pages 1995–2002, 2013.
- [12] M. Fumero, F. Wenzel, L. Zancato, A. Achille, E. Rodolà, S. Soatto, B. Schölkopf, and F. Locatello. Leveraging sparse and shared feature activations for disentangled representation learning. *Advances in Neural Information Processing Systems*, 36:27682–27698, 2023.
- [13] C. Glymour, K. Zhang, and P. Spirtes. Review of causal discovery methods based on graphical models. *Frontiers in genetics*, 10:524, 2019.

- [14] L. Gresele, P. K. Rubenstein, A. Mehrjou, F. Locatello, and B. Schölkopf. The incomplete rosetta stone problem: Identifiability results for multi-view nonlinear ica. In *Uncertainty in Artificial Intelligence*, pages 217–227. PMLR, 2020.
- [15] G. L. Gropper. Why is a picture worth a thousand words? *Audio Visual Communication Review*, 11(4): 75–95, 1963.
- [16] M. Gutmann and A. Hyvärinen. Noise-contrastive estimation: A new estimation principle for unnormalized statistical models. In *Proceedings of the thirteenth international conference on artificial intelligence and statistics*, pages 297–304. JMLR Workshop and Conference Proceedings, 2010.
- [17] X. He and Y. Peng. Fine-grained image classification via combining vision and language. In *Proceedings of the IEEE Conference on Computer Vision and Pattern Recognition*, pages 5994–6002, 2017.
- [18] P. Helber, B. Bischke, A. Dengel, and D. Borth. Eurosat: A novel dataset and deep learning benchmark for land use and land cover classification. *IEEE Journal of Selected Topics in Applied Earth Observations and Remote Sensing*, 12(7):2217–2226, 2019.
- [19] D. Hendrycks, S. Basart, N. Mu, S. Kadavath, F. Wang, E. Dorundo, R. Desai, T. Zhu, S. Parajuli, M. Guo, D. Song, J. Steinhardt, and J. Gilmer. The many faces of robustness: A critical analysis of out-of-distribution generalization. *ICCV*, 2021.
- [20] D. Hendrycks, K. Zhao, S. Basart, J. Steinhardt, and D. Song. Natural adversarial examples. *CVPR*, 2021.
- [21] P. Hoyer, D. Janzing, J. M. Mooij, J. Peters, and B. Schölkopf. Nonlinear causal discovery with additive noise models. *Advances in neural information processing systems*, 21, 2008.
- [22] Y. Huang, C. Du, Z. Xue, X. Chen, H. Zhao, and L. Huang. What makes multi-modal learning better than single (provably). *Advances in Neural Information Processing Systems*, 34:10944–10956, 2021.
- [23] N. J. Hum, P. E. Chamberlin, B. L. Hambright, A. C. Portwood, A. C. Schat, and J. L. Bevan. A picture is worth a thousand words: A content analysis of facebook profile photographs. *Computers in Human Behavior*, 27(5):1828–1833, 2011.
- [24] A. Hyvärinen. Fast and robust fixed-point algorithms for independent component analysis. *IEEE transactions on Neural Networks*, 10(3):626–634, 1999.
- [25] A. Hyvärinen and H. Morioka. Unsupervised feature extraction by time-contrastive learning and nonlinear ica. *Advances in neural information processing systems*, 29, 2016.
- [26] A. Hyvärinen and H. Morioka. Nonlinear ica of temporally dependent stationary sources. In *Artificial Intelligence and Statistics*, pages 460–469. PMLR, 2017.
- [27] A. Hyvärinen and P. Pajunen. Nonlinear independent component analysis: Existence and uniqueness results. *Neural networks*, 12(3):429–439, 1999.
- [28] A. Hyvärinen, J. Karhunen, and E. Oja. *Independent Component Analysis*. Adaptive and Cognitive Dynamic Systems: Signal Processing, Learning, Communications and Control. Wiley, 2001.
- [29] A. Hyvärinen, H. Sasaki, and R. Turner. Nonlinear ica using auxiliary variables and generalized contrastive learning. In *The 22nd International Conference on Artificial Intelligence and Statistics*, pages 859–868. PMLR, 2019.
- [30] H. Jiang. Uniform convergence rates for kernel density estimation. In *International Conference on Machine Learning*, pages 1694–1703. PMLR, 2017.
- [31] Y. Jiang, Z. Huang, X. Pan, C. C. Loy, and Z. Liu. Talk-to-edit: Fine-grained facial editing via dialog. In *Proceedings of International Conference on Computer Vision (ICCV)*, 2021.
- [32] I. Khemakhem, D. Kingma, R. Monti, and A. Hyvärinen. Variational autoencoders and nonlinear ica: A unifying framework. In *International Conference on Artificial Intelligence and Statistics*, pages 2207–2217. PMLR, 2020.
- [33] H. Kim and A. Mnih. Disentangling by factorising. In *International Conference on Machine Learning*, pages 2649–2658. PMLR, 2018.
- [34] J. Krause, M. Stark, J. Deng, and L. Fei-Fei. 3d object representations for fine-grained categorization. In *Proceedings of the IEEE international conference on computer vision workshops*, pages 554–561, 2013.

- [35] V. W. Liang, Y. Zhang, Y. Kwon, S. Yeung, and J. Y. Zou. Mind the gap: Understanding the modality gap in multi-modal contrastive representation learning. *Advances in Neural Information Processing Systems*, 35:17612–17625, 2022.
- [36] P. Lippe, S. Magliacane, S. Löwe, Y. M. Asano, T. Cohen, and S. Gavves. Citris: Causal identifiability from temporal intervened sequences. In *International Conference on Machine Learning*, pages 13557–13603. PMLR, 2022.
- [37] Y. Liu, Z. Zhang, D. Gong, M. Gong, B. Huang, A. van den Hengel, K. Zhang, and J. Q. Shi. Identifiable latent polynomial causal models through the lens of change. In *The Twelfth International Conference on Learning Representations*, 2024.
- [38] Z. Liu, P. Luo, X. Wang, and X. Tang. Deep learning face attributes in the wild. In *Proceedings of International Conference on Computer Vision (ICCV)*, December 2015.
- [39] T. Lüddecke and A. Ecker. Image segmentation using text and image prompts. In *Proceedings of the IEEE/CVF Conference on Computer Vision and Pattern Recognition*, pages 7086–7096, 2022.
- [40] S. Maji, E. Rahtu, J. Kannala, M. Blaschko, and A. Vedaldi. Fine-grained visual classification of aircraft. *arXiv preprint arXiv:1306.5151*, 2013.
- [41] R. Nakada, H. I. Gulluk, Z. Deng, W. Ji, J. Zou, and L. Zhang. Understanding multimodal contrastive learning and incorporating unpaired data. In *International Conference on Artificial Intelligence and Statistics*, pages 4348–4380. PMLR, 2023.
- [42] M.-E. Nilsback and A. Zisserman. Automated flower classification over a large number of classes. In *2008 Sixth Indian conference on computer vision, graphics & image processing*, pages 722–729. IEEE, 2008.
- [43] A. v. d. Oord, Y. Li, and O. Vinyals. Representation learning with contrastive predictive coding. *arXiv preprint arXiv:1807.03748*, 2018.
- [44] O. M. Parkhi, A. Vedaldi, A. Zisserman, and C. Jawahar. Cats and dogs. In *2012 IEEE conference on computer vision and pattern recognition*, pages 3498–3505. IEEE, 2012.
- [45] J. Pearl. *Causality: Models, Reasoning, and Inference*. Cambridge University Press, Cambridge, 2000.
- [46] J. Peters, J. M. Mooij, D. Janzing, and B. Schölkopf. Causal discovery with continuous additive noise models. *Journal of Machine Learning Research*, 2014.
- [47] A. Radford, J. W. Kim, C. Hallacy, A. Ramesh, G. Goh, S. Agarwal, G. Sastry, A. Askell, P. Mishkin, J. Clark, et al. Learning transferable visual models from natural language supervision. In *International conference on machine learning*, pages 8748–8763. PMLR, 2021.
- [48] B. Recht, R. Roelofs, L. Schmidt, and V. Shankar. Do imagenet classifiers generalize to imagenet? In *International conference on machine learning*, pages 5389–5400. PMLR, 2019.
- [49] H. Reinert. One picture is worth a thousand words? not necessarily! *Modern Language Journal*, pages 160–168, 1976.
- [50] N. Saunshi, O. Plevrakis, S. Arora, M. Khodak, and H. Khandeparkar. A theoretical analysis of contrastive unsupervised representation learning. In *International Conference on Machine Learning*, pages 5628–5637. PMLR, 2019.
- [51] B. Schölkopf, F. Locatello, S. Bauer, N. R. Ke, N. Kalchbrenner, A. Goyal, and Y. Bengio. Toward causal representation learning. *Proceedings of the IEEE*, 109(5):612–634, 2021.
- [52] A. Seigal, C. Squires, and C. Uhler. Linear causal disentanglement via interventions. *arXiv preprint arXiv:2211.16467*, 2022.
- [53] S. Shimizu, P. O. Hoyer, A. Hyvärinen, A. Kerminen, and M. Jordan. A linear non-gaussian acyclic model for causal discovery. *Journal of Machine Learning Research*, 7(10), 2006.
- [54] K. Soomro, A. R. Zamir, and M. Shah. Ucf101: A dataset of 101 human actions classes from videos in the wild. *arXiv preprint arXiv:1212.0402*, 2012.
- [55] P. Spirtes, C. Glymour, and R. Scheines. *Causation, Prediction, and Search*. MIT Press, Cambridge, MA, 2nd edition, 2001.

- [56] Y. Tian, D. Krishnan, and P. Isola. Contrastive multiview coding. In *Computer Vision–ECCV 2020: 16th European Conference, Glasgow, UK, August 23–28, 2020, Proceedings, Part XI* 16, pages 776–794. Springer, 2020.
- [57] B. Varici, E. Acarturk, K. Shanmugam, A. Kumar, and A. Tajer. Score-based causal representation learning with interventions. *arXiv preprint arXiv:2301.08230*, 2023.
- [58] J. Von Kügelgen, Y. Sharma, L. Gresele, W. Brendel, B. Schölkopf, M. Besserve, and F. Locatello. Self-supervised learning with data augmentations provably isolates content from style. *Advances in neural information processing systems*, 34:16451–16467, 2021.
- [59] H. Wang, S. Ge, Z. Lipton, and E. P. Xing. Learning robust global representations by penalizing local predictive power. In *Advances in Neural Information Processing Systems*, pages 10506–10518, 2019.
- [60] T. Wang and P. Isola. Understanding contrastive representation learning through alignment and uniformity on the hypersphere. In *International Conference on Machine Learning*, pages 9929–9939. PMLR, 2020.
- [61] J. Xiao, J. Hays, K. A. Ehinger, A. Oliva, and A. Torralba. Sun database: Large-scale scene recognition from abbey to zoo. In *2010 IEEE computer society conference on computer vision and pattern recognition*, pages 3485–3492. IEEE, 2010.
- [62] D. Yao, D. Xu, S. Lachapelle, S. Magliacane, P. Taslakian, G. Martius, J. von Kügelgen, and F. Locatello. Multi-view causal representation learning with partial observability. *arXiv preprint arXiv:2311.04056*, 2023.
- [63] R. Zhang, W. Zhang, R. Fang, P. Gao, K. Li, J. Dai, Y. Qiao, and H. Li. Tip-adapter: Training-free adaption of clip for few-shot classification. In *European conference on computer vision*, pages 493–510. Springer, 2022.
- [64] Y. Zhang, H. Jiang, Y. Miura, C. D. Manning, and C. P. Langlotz. Contrastive learning of medical visual representations from paired images and text. In *Machine Learning for Healthcare Conference*, pages 2–25. PMLR, 2022.
- [65] K. Zhou, J. Yang, C. C. Loy, and Z. Liu. Conditional prompt learning for vision-language models. In *Proceedings of the IEEE/CVF Conference on Computer Vision and Pattern Recognition*, pages 16816–16825, 2022.
- [66] K. Zhou, J. Yang, C. C. Loy, and Z. Liu. Learning to prompt for vision-language models. *International Journal of Computer Vision*, 130(9):2337–2348, 2022.
- [67] R. S. Zimmermann, Y. Sharma, S. Schneider, M. Bethge, and W. Brendel. Contrastive learning inverts the data generating process. In *International Conference on Machine Learning*, pages 12979–12990. PMLR, 2021.

Appendix

Table of Contents

A	Related Work	15
B	The Proof of Theorem 3.1	16
C	Relation with Recovering All Information	16
D	The Proof of identifiability on hypersphere	17
D.1	The Proof of Theorem 4.1	17
D.2	Identifiability result on hypersphere	19
E	The Proof of identifiability on convex bodies	19
E.1	The Proof of Theorem 4.3	19
E.2	Identifiability result on Convex Bodies	21
F	Differences from Previous Analysis for Multimodal Contrastive Learning	22
G	Differences from Previous Analyses for Single-Modal Contrastive Learning	22
H	More Results on CelebA	24
I	More Results on ImageNet-Type Data	26
J	More Results on Few-Shot Learning Task	27
K	Implementation Details	29

A Related Work

Multimodal contrastive representation learning Multi-modal contrastive representation learning, driven by underlying transferable knowledge across modalities, aims to coalesce inputs from these diverse sources into a cohesive representation space. This is typically achieved using a symmetric version of the standard contrastive loss [43, 16], a method designed to align accurate pairings while distinguishing incorrect ones [17, 47]. Although this approach has proven successful in a range of downstream tasks [47, 65, 66, 39, 2], there remains a gap in our comprehensive theoretical and empirical understanding of the representations it learns. Recently, there has been a growing interest in exploring multi-modal contrastive learning from various perspectives. For instance, the study by [35] provides insights into the modality gap inherent in multi-modal contrastive learning. Similarly, the research presented by [41] establishes a link between general multimodal contrastive loss and SVD analysis. Additionally, [22] posits that learning with multiple modalities can lead to a reduced population risk compared to using a subset of these modalities. Diverging from these approaches, our work delves into multi-modal contrastive representation learning by examining its connection with generative models.

Past research has sought to comprehend the representations derived from standard single-modality contrastive learning, examining them through the lens of alignment and uniformity [60], showing guarantees on the performance of the learned representations on the average classification task [50], or in terms of the identifiability of latent variables [67, 58]. Building on these foundations, our work takes a foreword step. We demonstrate that multi-modal contrastive learning can identify latent coupled variables, extending the insights from previous studies into the realm of multi-modality. Refer to Section G for more details.

Very recently, several studies have emerged, focusing on multi-modal settings [8, 62]. A clear distinction is that: the proposed model captures transferable knowledge across modalities by an undirected edge between latent coupled variables, while previous works often achieve it by introducing shared variables [8, 62]. Notably, our modeling approach is more general, as it can be reduced to the shared variables used in previous works [8, 62] by enforcing an identical mapping on the undirected edge between latent coupled variables. Some of these works have only achieved partial identifiability of coupled variables [8, 62], specifically identifying latent content variables but not latent style variables. In contrast, our work achieves comprehensive identifiability results for all latent coupled variables, offering a deeper level of understanding. Our research also diverges from the approach taken in [14] in two key ways: Firstly, we model transferable knowledge across modalities using conditional distributions, whereas the latter utilizes identical variables for this purpose. Secondly, while [14] relies on the premise that the mapping from the latent space to observations must be constrained by component-wise corrupters to ensure identifiability, our findings do not necessitate such constraints. Refer to Section F for more details.

Nonlinear ICA Nonlinear Independent Component Analysis (ICA) aims to unravel latent independent variables from observational data that has been subject to a nonlinear mixture of these latent factors. However, as pointed out in the seminal work by [27], solving this problem is generally infeasible without specific underlying assumptions. A prominent direction in contemporary research leverages the concept of distributional changes in latent variables, which leads to the creation of multi-domain observational data. This approach has been extensively explored and developed in a series of studies [25, 26, 29, 32], each contributing to a deeper understanding and more refined methodologies in the field of Nonlinear ICA. We build upon this body of research by incorporating co-occurrence patterns observed across multiple modalities. It is important to note the distinct difference between multi-domain and multi-modal approaches. The former typically implies a consistent mapping from the latent space to the observational space across all domains, whereas the latter accommodates different mappings for each modality. Additionally, while multi-domain approaches generally assume a totally shared latent variables across all domains, multi-modal methods allow for the existence of modality-specific latent variables.

B The Proof of Theorem 3.1

Theorem 2.1. (The asymptotics of \mathcal{L}) For fixed $\tau > 0$, as the sample size $N \rightarrow \infty$, the (normalized) multimodal contrastive loss converges to

$$\begin{aligned} \lim_{N \rightarrow \infty} \mathcal{L} - 2 \log N = & 2 \mathbb{E}_{(\mathbf{x}, \mathbf{t}) \sim p(\mathbf{x}, \mathbf{t})} [d(\mathbf{f}_x(\mathbf{x}), \mathbf{f}_t(\mathbf{t})) / \tau] + \mathbb{E}_{\mathbf{x} \sim p(\mathbf{x})} \left[\log \mathbb{E}_{\mathbf{t} \sim p(\mathbf{t})} [e^{-d(\mathbf{f}_x(\mathbf{x}), \mathbf{f}_t(\mathbf{t})) / \tau}] \right] \\ & + \mathbb{E}_{\mathbf{t} \sim p(\mathbf{t})} \left[\log \mathbb{E}_{\mathbf{x} \sim p(\mathbf{x})} [e^{-d(\mathbf{f}_x(\mathbf{x}), \mathbf{f}_t(\mathbf{t})) / \tau}] \right]. \end{aligned} \quad (10)$$

Proof. This proof is done by mainly depending on the Continuous Mapping Theorem and the law of large numbers.

$$\begin{aligned} \lim_{N \rightarrow \infty} \mathcal{L} - 2 \log N &= \lim_{N \rightarrow \infty} \left(-\frac{1}{N} \sum_{i=1}^N \log \frac{e^{-d(\mathbf{f}_x(\mathbf{x}_i), \mathbf{f}_t(\mathbf{t}_i)) / \tau}}{\sum_{j=1}^N e^{-d(\mathbf{f}_x(\mathbf{x}_i), \mathbf{f}_t(\mathbf{t}_j)) / \tau}} \right. \\ &\quad \left. - \frac{1}{N} \sum_{i=1}^N \log \frac{e^{-d(\mathbf{f}_x(\mathbf{x}_i), \mathbf{f}_t(\mathbf{t}_i)) / \tau}}{\sum_{j=1}^N e^{-d(\mathbf{f}_x(\mathbf{x}_j), \mathbf{f}_t(\mathbf{t}_i)) / \tau}} \right) - 2 \log N, \\ &= \lim_{N \rightarrow \infty} \left(\frac{2}{N} \sum_{i=1}^N d(\mathbf{f}_x(\mathbf{x}_i), \mathbf{f}_t(\mathbf{t}_i)) / \tau + \frac{1}{N} \sum_{i=1}^N \log \sum_{j=1}^N e^{-d(\mathbf{f}_x(\mathbf{x}_i), \mathbf{f}_t(\mathbf{t}_j)) / \tau} \right. \\ &\quad \left. + \frac{1}{N} \sum_{i=1}^N \log \sum_{j=1}^N e^{-d(\mathbf{f}_x(\mathbf{x}_j), \mathbf{f}_t(\mathbf{t}_i)) / \tau} \right) - 2 \log N \\ &= \lim_{N \rightarrow \infty} \left(\frac{2}{N} \sum_{i=1}^N d(\mathbf{f}_x(\mathbf{x}_i), \mathbf{f}_t(\mathbf{t}_i)) / \tau + \frac{1}{N} \sum_{i=1}^N \log \frac{1}{N} \sum_{j=1}^N e^{-d(\mathbf{f}_x(\mathbf{x}_i), \mathbf{f}_t(\mathbf{t}_j)) / \tau} \right. \\ &\quad \left. + \frac{1}{N} \sum_{i=1}^N \log \frac{1}{N} \sum_{j=1}^N e^{-d(\mathbf{f}_x(\mathbf{x}_j), \mathbf{f}_t(\mathbf{t}_i)) / \tau} + \frac{2}{N} \sum_{i=1}^N \log N \right) - 2 \log N \\ &= 2 \mathbb{E}_{(\mathbf{x}, \mathbf{t}) \sim p(\mathbf{x}, \mathbf{t})} [d(\mathbf{f}_x(\mathbf{x}), \mathbf{f}_t(\mathbf{t})) / \tau] + \mathbb{E}_{\mathbf{x} \sim p(\mathbf{x})} \left[\log \mathbb{E}_{\mathbf{t} \sim p(\mathbf{t})} [e^{-d(\mathbf{f}_x(\mathbf{x}), \mathbf{f}_t(\mathbf{t})) / \tau}] \right] \\ &\quad + \mathbb{E}_{\mathbf{t} \sim p(\mathbf{t})} \left[\log \mathbb{E}_{\mathbf{x} \sim p(\mathbf{x})} [e^{-d(\mathbf{f}_x(\mathbf{x}), \mathbf{f}_t(\mathbf{t})) / \tau}] \right]. \end{aligned}$$

□

C Relation with Recovering All Information

In this section, we proof

$$\begin{aligned} & \mathbb{E}_{\mathbf{x} \sim p(\mathbf{x})} \left[\log \mathbb{E}_{\mathbf{t} \sim p(\mathbf{t})} [e^{-d(\mathbf{f}_x(\mathbf{x}), \mathbf{f}_t(\mathbf{t})) / \tau}] \right] + \mathbb{E}_{\mathbf{t} \sim p(\mathbf{t})} \left[\log \mathbb{E}_{\mathbf{x} \sim p(\mathbf{x})} [e^{-d(\mathbf{f}_x(\mathbf{x}), \mathbf{f}_t(\mathbf{t})) / \tau}] \right] \\ & \approx -H(p(\mathbf{f}_x(\mathbf{x})), p(\mathbf{f}_t(\mathbf{t}))) - H(p(\mathbf{f}_t(\mathbf{t})), p(\mathbf{f}_x(\mathbf{x}))). \end{aligned}$$

Considering the symmetry evident in both the left and right sides of the equation, let us focus our attention on the initial term on the left and its corresponding counterpart on the right.

$$\begin{aligned} & \mathbb{E}_{\mathbf{x} \sim p(\mathbf{x})} \left[\log \mathbb{E}_{\mathbf{t} \sim p(\mathbf{t})} [e^{-d(\mathbf{f}_x(\mathbf{x}), \mathbf{f}_t(\mathbf{t})) / \tau}] \right] \\ &= \lim_{N \rightarrow \infty} \frac{1}{N} \sum_{i=1}^N \log \frac{1}{N} \sum_{j=1}^N e^{-d(\mathbf{f}_x(\mathbf{x}_i), \mathbf{f}_t(\mathbf{t}_j)) / \tau} \end{aligned} \quad (11)$$

$$\approx \lim_{N \rightarrow \infty} \frac{1}{N} \sum_{i=1}^N \log p_{\text{KDE}}(\mathbf{f}_x(\mathbf{x}_i)) + \log Z_{\text{KDE}} \quad (12)$$

$$= -H(p(\mathbf{f}_x(\mathbf{x})), p(\mathbf{f}_t(\mathbf{t}))) + \log Z_{\text{KDE}}, \quad (13)$$

Transitioning from Eq. (11) to Eq. (12), we employ kernel density estimation, wherein the choice of kernel is influenced by the distance metric used. For instance, on a hypersphere, a von Mises-Fisher kernel is suitable, whereas on convex bodies, a Laplace kernel aligns well with the L1 norm. In this context, $\log Z_{\text{KDE}}$ represents

the normalization constant associated with the kernel. The inherent symmetry in this setup allows us to logically deduce the equation. Note that since here the bandwidth τ can be optimized in multimodal contrastive representation learning, if true distribution is the same as the chosen kernel, Eq. (12) is equal to Eq. (11), i.e., \approx in Eq. (12) can be $=$. Under certain conditions the kernel density estimation will converge to the real distribution, in that case \approx in Eq. (12) can also be $=$.

D The Proof of identifiability on hypersphere

D.1 The Proof of Theorem 4.1

Theorem 3.1. (\mathcal{L} converges to the symmetric cross-entropy) *Under the assumptions defined in Eq. (4) for the proposed latent partial causal model, the necessary condition $\mathbf{f}_x \circ \mathbf{g}_x = \mathbf{f}_t \circ \mathbf{g}_t$, denoted as \mathbf{h} , for the optimal normalized multimodal contrastive loss given by Eq. (2) leads to the following reduction of the loss itself:*

$$\lim_{N \rightarrow \infty} \mathcal{L} - 2 \log N = \mathbb{E}_{\mathbf{z}_x \sim p(\mathbf{z}_x)} [H(p(\mathbf{z}_t|\mathbf{z}_x), q_{\mathbf{h}}(\mathbf{z}_t|\mathbf{z}_x))] + \mathbb{E}_{\mathbf{z}_t \sim p(\mathbf{z}_t)} [H(p(\mathbf{z}_x|\mathbf{z}_t), q_{\mathbf{h}}(\mathbf{z}_x|\mathbf{z}_t))] \quad (14)$$

where H is the cross entropy, the conditional distributions $q_{\mathbf{h}}(\mathbf{z}_t|\mathbf{z}_x)$ and $q(\mathbf{z}_x|\mathbf{z}_t)$ are parameterized by the following:

$$q_{\mathbf{h}}(\mathbf{z}_t|\mathbf{z}_x) = C_q(\mathbf{z}_t)^{-1} e^{(\mathbf{h}(\mathbf{z}_x)^T \mathbf{h}(\mathbf{z}_t)/\tau)}, \quad (15)$$

$$q_{\mathbf{h}}(\mathbf{z}_t|\mathbf{z}_x) = C_q(\mathbf{z}_x)^{-1} e^{(\mathbf{h}(\mathbf{z}_t)^T \mathbf{h}(\mathbf{z}_x)/\tau)}, \quad (16)$$

with

$$C_q(\mathbf{z}_t) = \int e^{(\mathbf{h}(\mathbf{z}_x)^T \mathbf{h}(\mathbf{z}_t)/\tau)} d\mathbf{z}_x,$$

$$C_q(\mathbf{z}_x) = \int e^{(\mathbf{h}(\mathbf{z}_x)^T \mathbf{h}(\mathbf{z}_t)/\tau)} d\mathbf{z}_t.$$

To proof Theorem 4.1, we first introduce the following Lemma.

Lemma 4.1. *Consider the unit hypersphere space, given uniform prior $p(\mathbf{z}_x)$, $p(\mathbf{z}_x) = |\mathcal{Z}|^{-1}$ where $\mathcal{Z} \subseteq \mathbb{R}^M$ denotes the space of \mathbf{z}_x , and conditional distribution $p(\mathbf{z}_t|\mathbf{z}_x) = C_p(k) \exp(k\mathbf{z}_x^T \mathbf{z}_t)$, $p(\mathbf{z}_t)$ follows a uniform distribution.*

Proof. By Bayesian theorem, $p(\mathbf{z}_t) = \int p(\mathbf{z}_t|\mathbf{z}_x)p(\mathbf{z}_x)d\mathbf{z}_x = |\mathcal{Z}|^{-1} \int p(\mathbf{z}_t|\mathbf{z}_x)d\mathbf{z}_x = |\mathcal{Z}|^{-1} C_p(k) \int \exp(k\mathbf{z}_x^T \mathbf{z}_t) d\mathbf{z}_x$, then due to the unit hypersphere space, we have $\int \exp(k\mathbf{z}_x^T \mathbf{z}_t) d\mathbf{z}_x = C_p(k)^{-1}$. As a result, we obtain $p(\mathbf{z}_t) = |\mathcal{Z}|^{-1}$. \square

Lemma 5.1. *The normalized multimodal contrastive loss in Eq. (2) has an optimal global solution of 0, which can be attained under the following conditions:*

- $\mathbf{h}_x(\mathbf{m}_x, \mathbf{z}_x) = \mathbf{h}_t(\mathbf{m}_t, \mathbf{z}_t)$ almost surely, for pair $((\mathbf{m}_x, \mathbf{z}_x), (\mathbf{m}_t, \mathbf{z}_t))$, (C1),
- \mathbf{h}_x and \mathbf{h}_t map $(\mathbf{m}_x, \mathbf{z}_x)$ and $(\mathbf{m}_t, \mathbf{z}_t)$, respectively, to uniform variables on hypersphere, (C2),

Proof. First, it is well known that traditional contrastive loss in single modality has an optimal global solution of $\log N$ [43, 56], as a result, the multimodal contrastive loss Eq. 1 has an optimal global solution of $2 \log N$. For completeness, let us focus on the first term in Eq. 1:

$$-\frac{1}{N} \sum_{i=1}^N \log \frac{e^{-d(\mathbf{f}_x(\mathbf{x}_i), \mathbf{f}_t(\mathbf{t}_i))/\tau}}{\sum_{j=1}^N e^{-d(\mathbf{f}_x(\mathbf{x}_i), \mathbf{f}_t(\mathbf{t}_j))/\tau}}, \quad (17)$$

Under optimal contrastive learning conditions, the distance for positive pairs satisfies: $e^{-d(\mathbf{f}_x(\mathbf{x}_i), \mathbf{f}_t(\mathbf{t}_i))/\tau} = 1$, for negative pairs $(\mathbf{x}_i, \mathbf{x}_j)$ where $i \neq j$: $e^{-d(\mathbf{f}_x(\mathbf{x}_i), \mathbf{f}_t(\mathbf{t}_j))/\tau} = \epsilon$, where ϵ is a small value. As a result, for each i , the denominator can be expressed as: $1 + (N-1)\epsilon$. Therefore, the first term in Eq. 1 reduces to: $-\frac{1}{N} \sum_{i=1}^N \log \frac{1}{1+(N-1)\epsilon}$. Clearly, when N is large, the first term in Eq. 1 equals to $\log N$. Given that the second term is symmetric, we conclude that Eq. 1 has an optimal global solution of $2 \log N$. Therefore, Eq. 10 achieves a global optimal solution of 0. To reach the global minimum of 0, we observe that the first term in Eq. 10 is minimized if and only if $\mathbf{h}_x(\mathbf{m}_x, \mathbf{z}_x) = \mathbf{h}_t(\mathbf{m}_t, \mathbf{z}_t)$ almost surely, for real pair $((\mathbf{m}_x, \mathbf{z}_x), (\mathbf{m}_t, \mathbf{z}_t))$, (marked as (C1)). Thus, we obtain a minimum solution of 0 for the first term. Next, considering the remaining two terms in Eq. 10, as detailed in Appendix C, we see an equivalent expression: $-H(p(\mathbf{f}_x(\mathbf{x}), p(\mathbf{f}_t(\mathbf{t}))) - H(p(\mathbf{f}_x(\mathbf{x}), p(\mathbf{f}_t(\mathbf{t}))) + 2 \log Z_{\text{KDE}}$. When both \mathbf{h}_x and \mathbf{h}_t map $(\mathbf{m}_x, \mathbf{z}_x)$ and $(\mathbf{m}_t, \mathbf{z}_t)$, respectively, to

uniform variables on hypersphere (marked as (C2)), it reduces to $-2H(p(\mathbf{f}_x(\mathbf{x})) + 2\log Z_{\text{KDE}}$. Note that the entropy of a uniform distribution on the hypersphere \mathbb{S}^{M-1} is $\log(\frac{2\pi^{M/2}}{\Gamma(M/2)})$, where Γ is the gamma function. Together with the fact that the normalization constant of uniform distribution on hypersphere is $\log(\frac{2\pi^{M/2}}{\Gamma(M/2)})$ (i.e., $\log Z_{\text{KDE}}$), we arrive at the optimal solution of 0 for the last two terms. \square

Proof sketch The proof of Theorem 4.1 hinges on demonstrating the equality between the right-hand side of Eq. (14) and Eq. (10). Let us define $\mathbf{h}_x = \mathbf{f}_x \circ \mathbf{g}_x$ and $\mathbf{h}_t = \mathbf{f}_t \circ \mathbf{g}_t$. In Step I, using Lemma 5.1, we show that (1) $\mathbf{f}_x \circ \mathbf{g}_x = \mathbf{f}_t \circ \mathbf{g}_t$, and (2) they are independent of the modality-specific variables \mathbf{m}_x and \mathbf{m}_t . In Step II, by defining $\mathbf{h} = \mathbf{f}_x \circ \mathbf{g}_x = \mathbf{f}_t \circ \mathbf{g}_t$ and applying both the generative model from Eq. (4) and the inference model from Eqs. (15)-(16), we establish the theorem.

Step I Consider C1 in Lemma 5.1, e.g., $\mathbf{h}_x(\mathbf{m}_x, \mathbf{z}_x) = \mathbf{h}_t(\mathbf{m}_t, \mathbf{z}_t)$ almost surely, for pair $((\mathbf{m}_x, \mathbf{z}_x), (\mathbf{m}_t, \mathbf{z}_t))$, by differentiating it with respect to \mathbf{m}_x , we have:

$$\frac{\partial \mathbf{h}_x(\mathbf{m}_x, \mathbf{z}_x)}{\partial \mathbf{m}_x} = \frac{\partial \mathbf{h}_t(\mathbf{m}_t, \mathbf{z}_t)}{\partial \mathbf{m}_x} = 0, \quad (18)$$

, due to the independence between \mathbf{m}_x and $(\mathbf{m}_t, \mathbf{z}_t)$. Similarly, by differentiating it with respect to \mathbf{m}_t , we have:

$$\frac{\partial \mathbf{h}_t(\mathbf{m}_t, \mathbf{z}_t)}{\partial \mathbf{m}_t} = \frac{\partial \mathbf{h}_x(\mathbf{m}_x, \mathbf{z}_x)}{\partial \mathbf{m}_t} = 0. \quad (19)$$

Based on Eqs. (18) and (19), we conclude that both \mathbf{h}_x and \mathbf{h}_t are independent of the modality-specific variables \mathbf{m}_x and \mathbf{m}_t , respectively, i.e., $\mathbf{h}_x(\mathbf{m}_x, \mathbf{z}_x) = \mathbf{h}_x(\mathbf{z}_x)$ and $\mathbf{h}_t(\mathbf{m}_t, \mathbf{z}_t) = \mathbf{h}_t(\mathbf{z}_t)$. As a result, we have $\mathbf{h}_x(\mathbf{z}_x) = \mathbf{h}_t(\mathbf{z}_t)$, for all real pairs $(\mathbf{z}_x, \mathbf{z}_t)$ sampled from the conditional distribution $p(\mathbf{z}_t|\mathbf{z}_x)$ defined in Eq. (4). Note that this expression also holds true for $\mathbf{z}_t = \mathbf{z}_x$ (e.g., when \mathbf{z}_t is sampled with the same value as \mathbf{z}_x), which implies $\mathbf{h}_x(\mathbf{z}_x) = \mathbf{h}_t(\mathbf{z}_x)$. As a result, we can obtain: $\mathbf{h}_x = \mathbf{h}_t$.

Step II According to the results above: $\mathbf{h}_x(\mathbf{m}_x, \mathbf{z}_x) = \mathbf{h}_x(\mathbf{z}_x)$, $\mathbf{h}_t(\mathbf{m}_t, \mathbf{z}_t) = \mathbf{h}_t(\mathbf{z}_x)$, and $\mathbf{h}_x = \mathbf{h}_t$ from Step I, by defining $\mathbf{h} \stackrel{\text{def}}{=} \mathbf{h}_x = \mathbf{h}_t$, we can rewrite Eq. (10) as:

$$2 \mathbb{E}_{(\mathbf{z}_x, \mathbf{z}_t) \sim p(\mathbf{z}_x, \mathbf{z}_t)} [d(\mathbf{h}(\mathbf{z}_x), \mathbf{h}(\mathbf{z}_t))/\tau] + \mathbb{E}_{\mathbf{z}_x \sim p(\mathbf{z}_x)} \left[\log \mathbb{E}_{\mathbf{z}_t \sim p(\mathbf{z}_t)} [e^{-d(\mathbf{h}(\mathbf{z}_x), \mathbf{h}(\mathbf{z}_t))/\tau}] \right] \\ + \mathbb{E}_{\mathbf{z}_t \sim p(\mathbf{z}_t)} \left[\log \mathbb{E}_{\mathbf{z}_x \sim p(\mathbf{z}_x)} [e^{-d(\mathbf{h}(\mathbf{z}_x), \mathbf{h}(\mathbf{z}_t))/\tau}] \right]. \quad (20)$$

We then connect the right-hand side of Eq. (14) with Eq. (20). To this end, since the two terms in the right-hand side of Eq. (14) are symmetrical, we focus on one of the two terms for convenience, e.g., $\mathbb{E}_{\mathbf{z}_x \sim p(\mathbf{z}_x)} [H(p(\mathbf{z}_t|\mathbf{z}_x)), q_{\mathbf{h}}(\mathbf{z}_t|\mathbf{z}_x)]$. Based on Lemma 4.1, it can be shown that:

$$\mathbb{E}_{\mathbf{z}_x \sim p(\mathbf{z}_x)} [H(p(\mathbf{z}_t|\mathbf{z}_x)), q_{\mathbf{h}}(\mathbf{z}_t|\mathbf{z}_x)] \quad (21)$$

$$= \mathbb{E}_{\mathbf{z}_x \sim p(\mathbf{z}_x)} \left[\mathbb{E}_{\mathbf{z}_t \sim p(\mathbf{z}_t|\mathbf{z}_x)} [-\log q_{\mathbf{h}}(\mathbf{z}_t|\mathbf{z}_x)] \right] \quad (22)$$

$$= \mathbb{E}_{(\mathbf{z}_x, \mathbf{z}_t) \sim p(\mathbf{z}_x, \mathbf{z}_t)} [-\mathbf{h}(\mathbf{z}_x)^T \mathbf{h}(\mathbf{z}_t)/\tau + \log C_q(\mathbf{z}_x)] \quad (23)$$

$$= \mathbb{E}_{(\mathbf{z}_x, \mathbf{z}_t) \sim p(\mathbf{z}_x, \mathbf{z}_t)} [-\mathbf{h}(\mathbf{z}_x)^T \mathbf{h}(\mathbf{z}_t)/\tau] + \mathbb{E}_{(\mathbf{z}_x) \sim p(\mathbf{z}_x)} [\log C_q(\mathbf{z}_x)] \quad (24)$$

$$= \mathbb{E}_{(\mathbf{z}_x, \mathbf{z}_t) \sim p(\mathbf{z}_x, \mathbf{z}_t)} [-\mathbf{h}(\mathbf{z}_x)^T \mathbf{h}(\mathbf{z}_t)/\tau] + \mathbb{E}_{(\mathbf{z}_x) \sim p(\mathbf{z}_x)} [\log \int e^{(\mathbf{h}(\mathbf{z}_x)^T \mathbf{h}(\mathbf{z}_t))/\tau} d\mathbf{z}_x] \quad (25)$$

Since $p(\mathbf{z}_x) = |\mathcal{Z}|^{-1}$, and $p(\mathbf{z}_t) = |\mathcal{Z}|^{-1}$ by Lemma 4.1, Eq. (25) simplifies to:

$$= - \mathbb{E}_{(\mathbf{z}_x, \mathbf{z}_t) \sim p(\mathbf{z}_x, \mathbf{z}_t)} [(\mathbf{h}(\mathbf{z}_x)^T \mathbf{h}(\mathbf{z}_t))/\tau] + \mathbb{E}_{\mathbf{z}_x \sim p(\mathbf{z}_x)} \left[\log \mathbb{E}_{\mathbf{z}_t \sim p(\mathbf{z}_t)} [e^{(\mathbf{h}(\mathbf{z}_x)^T \mathbf{h}(\mathbf{z}_t))/\tau}] \right] + \log |\mathcal{Z}| \quad (26)$$

On hypersphere space with radius r , due to $\|\mathbf{h}(\mathbf{z}_x) - \mathbf{h}(\mathbf{z}_t)\| = 2r - 2\mathbf{h}(\mathbf{z}_x)^T \mathbf{h}(\mathbf{z}_t)$, Eq. 26 simplifies to:

$$= \mathbb{E}_{(\mathbf{z}_x, \mathbf{z}_t) \sim p(\mathbf{z}_x, \mathbf{z}_t)} [d(\mathbf{h}(\mathbf{z}_x), \mathbf{h}(\mathbf{z}_t))/\tau] + \mathbb{E}_{\mathbf{z}_x \sim p(\mathbf{z}_x)} \left[\log \mathbb{E}_{\mathbf{z}_t \sim p(\mathbf{z}_t)} [e^{-d(\mathbf{h}(\mathbf{z}_x), \mathbf{h}(\mathbf{z}_t))/\tau}] \right] \quad (27)$$

Similarly, for the second term in the right-hand side of Eq. (14), we can proof that:

$$\begin{aligned}
\mathbb{E}_{(\mathbf{z}_t) \sim p(\mathbf{z}_t)} [H(p(\mathbf{z}_x|\mathbf{z}_t)), q_{\mathbf{h}}(\mathbf{z}_x|\mathbf{z}_t)] &= \mathbb{E}_{(\mathbf{z}_x, \mathbf{z}_t) \sim p(\mathbf{z}_x, \mathbf{z}_t)} [d(\mathbf{h}(\mathbf{z}_x), \mathbf{h}(\mathbf{z}_t))/\tau] \\
&+ \mathbb{E}_{\mathbf{z}_t \sim p(\mathbf{z}_t)} \left[\log \mathbb{E}_{\mathbf{z}_x \sim p(\mathbf{z}_x)} [e^{-d(\mathbf{h}(\mathbf{z}_x), \mathbf{h}(\mathbf{z}_t))/\tau}] \right] + \log |\mathcal{Z}|. \quad (28)
\end{aligned}$$

By combining Eq. (27) and Eq. (28), we can conclude the proof.

D.2 Identifiability result on hypersphere

Theorem 4.1 represents an adaptation of Theorem 1 from [67] in the context of multi-modal setting. Specifically, within the confines of a single-modal framework, Theorem 4.1 is consistent with the findings presented in Theorem 1 in [67]. Consequently, this alignment allows us to employ Propositions 1 and 2 from [67] to demonstrate that the global minimization of the objective outlined in Eq. (5), as specified in Theorem 4.1, identifies the latent variables \mathbf{z}_x , as well as \mathbf{z}_t , up to linear transformations. For completeness, a brief proof is provided herein, with comprehensive details available in the original work. Clearly, the global minimum of the cross-entropy between two distributions is reached if they match by value and have the same support. Therefore, for the optimal solution of the objective loss Eq. (14) in Theorem 4.1, we have:

$$p(\mathbf{z}_t|\mathbf{z}_x) = q_{\mathbf{h}}(\mathbf{z}_t|\mathbf{z}_x), \quad (29)$$

This expression also holds true for $\mathbf{z}_t = \mathbf{z}_x$; additionally using that \mathbf{h} maps from a unit hypersphere to one with radius $\sqrt{\tau}k$, we have:

$$\begin{aligned}
C_p^{-1} e^{(k\mathbf{z}_x^T \mathbf{z}_x)} &= C_q(\mathbf{z}_x)^{-1} e^{(\mathbf{h}(\mathbf{z}_x)^T \mathbf{h}(\mathbf{z}_x)/\tau)}, \\
\Leftrightarrow C_p &= C_q(\mathbf{z}_x) \quad (30)
\end{aligned}$$

As the normalization constants are identical we get for all $\mathbf{z}_x, \mathbf{z}_t$,

$$k\mathbf{z}_x^T \mathbf{z}_t = \mathbf{h}(\mathbf{z}_x)^T \mathbf{h}(\mathbf{z}_t)/\tau, \quad (31)$$

here we can see that \mathbf{h} maintains the dot product, which implies that \mathbf{h} must be an orthogonal linear transformation by using Proposition 2 in [67]. As a result, Theorem 4.1 is capable of identifying the latent variables \mathbf{z}_x and \mathbf{z}_t up to an orthogonal linear transformation, *i.e.*, the recovered latent variable $\mathbf{f}_x(\mathbf{x})$, obtained through the minimization of Eq. (5), is linearly related to the true \mathbf{z}_x as follows: $\mathbf{f}_x(\mathbf{x}) = \mathbf{A}\mathbf{z}_x + \mathbf{c}$, where \mathbf{A} represents an orthogonal matrix, and \mathbf{c} is a constant vector.

E The Proof of identifiability on convex bodies

E.1 The Proof of Theorem 4.3

Theorem 3.2. (\mathcal{L} converges to the symmetric cross-entropy) *Under the assumptions defined in Eq. (7) for the proposed latent partial causal model, the necessary condition $\mathbf{f}_x \circ \mathbf{g}_x = \mathbf{f}_t \circ \mathbf{g}_t$, denoted as \mathbf{h} , for the optimal normalized multimodal contrastive loss given by Eq. (2) leads to the following reduction of the loss itself:*

$$\lim_{N \rightarrow \infty} \mathcal{L} - 2 \log N = \mathbb{E}_{\mathbf{z}_x \sim p(\mathbf{z}_x)} [H(p(\mathbf{z}_t|\mathbf{z}_x)), q_{\mathbf{h}}(\mathbf{z}_t|\mathbf{z}_x)] + \mathbb{E}_{(\mathbf{z}_t) \sim p(\mathbf{z}_t)} [H(p(\mathbf{z}_x|\mathbf{z}_t)), q_{\mathbf{h}}(\mathbf{z}_x|\mathbf{z}_t)] \quad (32)$$

where H is the cross entropy, the conditional distributions $q_{\mathbf{h}}(\mathbf{z}_t|\mathbf{z}_x)$ and $q(\mathbf{z}_x|\mathbf{z}_t)$ are parameterized by the following:

$$q_{\mathbf{h}}(\mathbf{z}_x|\mathbf{z}_t) = C_q(\mathbf{z}_t)^{-1} e^{-\delta(\mathbf{h}(\mathbf{z}_x), \mathbf{h}(\mathbf{z}_t))/\tau}, \quad (33)$$

$$q_{\mathbf{h}}(\mathbf{z}_t|\mathbf{z}_x) = C_q(\mathbf{z}_x)^{-1} e^{-\delta(\mathbf{h}(\mathbf{z}_x), \mathbf{h}(\mathbf{z}_t))/\tau}, \quad (34)$$

with

$$\begin{aligned}
C_q(\mathbf{z}_t) &= \int e^{-\delta(\mathbf{h}(\mathbf{z}_x), \mathbf{h}(\mathbf{z}_t))/\tau} d\mathbf{z}_x, \\
C_q(\mathbf{z}_x) &= \int e^{-\delta(\mathbf{h}(\mathbf{z}_x), \mathbf{h}(\mathbf{z}_t))/\tau} d\mathbf{z}_t.
\end{aligned}$$

Similar to the proof D.1, we first introduce the following Lemma.

Lemma 4.2. *For random variables $\mathbf{z}_x \in \mathcal{Z}_c$ and $\mathbf{z}_t \in \mathcal{Z}_c$, assume that $p(\mathbf{z}_x) = 1/|\mathcal{Z}_c|$ if $\mathbf{z}_x \in \mathcal{Z}_c$ and 0 otherwise, and assume that conditional distribution $p(\mathbf{z}_t|\mathbf{z}_x) = C(\mathbf{z}_x) \exp(-\delta(\mathbf{z}_x, \mathbf{z}_t)/\lambda)$, where δ is a symmetric metric induced by a norm, then $p(\mathbf{z}_t)$ converges to uniform distribution on \mathcal{Z}_c as $\lambda \rightarrow 0_+$.*

Proof. The proof can be done by the fact that as $\lambda \rightarrow 0$, the condition distribution $p(\mathbf{z}_t|\mathbf{z}_x)$ converges to a delta distribution, resulting that $p(\mathbf{z}_t) = p(\mathbf{z}_x)$. More specifically, as we will let $\lambda \rightarrow 0$ in the procedure, it is notable that the normalize $C'(\mathbf{z}_x)$ actually depend on λ and should be write as $C'(\mathbf{z}_x, \lambda)$ in a more formal way. With simple integration trick, it would be straightforward to show that $C'(\mathbf{z}_x, \lambda)$ can be decomposed as $C'(\mathbf{z}_x, \lambda) = \frac{1}{\lambda} C'(\mathbf{z}_x)$.

By definition we have

$$\begin{aligned} p(\mathbf{z}_t) &= \int_{\mathbf{z}_x \in \mathcal{Z}_c} p(\mathbf{z}_x) p(\mathbf{z}_t|\mathbf{z}_x) d\mathbf{z}_x \\ &= \int_{\mathbf{z}_x \in \mathcal{Z}_c} p(\mathbf{z}_x) \frac{1}{\lambda} C'(\mathbf{z}_x) \exp(-\delta(\mathbf{z}_x, \mathbf{z}_t)/\lambda) d\mathbf{z}_x \\ &= \lim_{N \rightarrow +\infty} \sum_{i=1}^N \frac{1}{\lambda} C'(\mathbf{z}_{x_i}) \exp(-\delta(\mathbf{z}_{x_i}, \mathbf{z}_t)/\lambda), \forall i, \mathbf{z}_{x_i} \sim p(\mathbf{z}_x) \end{aligned} \quad (35)$$

then obviously we have that

$$\begin{aligned} \lim_{\lambda \rightarrow 0_+} p(\mathbf{z}_t) &= \lim_{\lambda \rightarrow 0_+} \lim_{N \rightarrow +\infty} \sum_{i=1}^N \frac{1}{\lambda} C'(\mathbf{z}_{x_i}) \exp(-\delta(\mathbf{z}_{x_i}, \mathbf{z}_t)/\lambda) \\ &= \lim_{\lambda \rightarrow 0_+} \lim_{N \rightarrow +\infty} \sum_{i=1}^N \frac{1}{\lambda} C' \exp(-\delta(\mathbf{z}_{x_i}, \mathbf{z}_t)/\lambda), \end{aligned} \quad (36)$$

where $C' = \int_{-\infty}^{\infty} \exp(-\delta(\mathbf{0}, \mathbf{z}_t)) d\mathbf{z}_t$. It is obvious that (36) can be viewed as a Kernel Density Estimation over samples $\mathbf{z}_{x_i} \sim p(\mathbf{z}_x)$, and obviously $\lim_{\tau \rightarrow 0_+} p(\mathbf{z}_t)$ will converge to $p(\mathbf{z}_x)$ (which is uniform distribution) under quite mild condition (for details of the convergence we refer to [30]). \square

Proof sketch Similar to hypersphere, the proof of Theorem 4.3 can be done by demonstrating that the right-hand side of Eq. (32) is equal to the right-hand side of Eq. (10) on convex bodies. To achieve this, using Lemma 5.1, we show that $\mathbf{f}_x \circ \mathbf{g}_x = \mathbf{f}_t \circ \mathbf{g}_t$, and they are independent of the modality-specific variables \mathbf{m}_x and \mathbf{m}_t , respectively. Finally, by defining $\mathbf{h} = \mathbf{f}_x \circ \mathbf{g}_x = \mathbf{f}_t \circ \mathbf{g}_t$, and using the inference model (33) and (34), we obtain our result.

Step I On convex bodies, and define $\mathbf{h}_x = \mathbf{f}_x \circ \mathbf{g}_x$ and $\mathbf{h}_t = \mathbf{f}_t \circ \mathbf{g}_t$. Consider C1 in Lemma 5.1, e.g., $\mathbf{h}_x(\mathbf{m}_x, \mathbf{z}_x) = \mathbf{h}_t(\mathbf{m}_t, \mathbf{z}_t)$ almost surely, for pair $((\mathbf{m}_x, \mathbf{z}_x), (\mathbf{m}_t, \mathbf{z}_t))$. Similar to Step I in Appendix D.1, by differentiating it with respect to \mathbf{m}_x and \mathbf{m}_t , respectively, we can conclude that both \mathbf{h}_x and \mathbf{h}_t are independent of the modality-specific variables \mathbf{m}_x and \mathbf{m}_t , respectively, i.e., $\mathbf{h}_x(\mathbf{m}_x, \mathbf{z}_x) = \mathbf{h}_x(\mathbf{z}_x)$ and $\mathbf{h}_t(\mathbf{m}_t, \mathbf{z}_t) = \mathbf{h}_t(\mathbf{z}_t)$. Further, since $\mathbf{h}_x(\mathbf{z}_x) = \mathbf{h}_t(\mathbf{z}_t)$ hold, for all real pairs $(\mathbf{z}_x, \mathbf{z}_t)$ sampled from the conditional distribution $p(\mathbf{z}_t|\mathbf{z}_x)$ defined in Eq. (7), this expression also holds true for $\mathbf{z}_t = \mathbf{z}_x$, which implies $\mathbf{h}_x(\mathbf{z}_x) = \mathbf{h}_t(\mathbf{z}_x)$. As a result, we can obtain: $\mathbf{h}_x = \mathbf{h}_t$.

Step II According to the results above: $\mathbf{h}_x(\mathbf{m}_x, \mathbf{z}_x) = \mathbf{h}_x(\mathbf{z}_x)$, $\mathbf{h}_t(\mathbf{m}_t, \mathbf{z}_t) = \mathbf{h}_t(\mathbf{z}_t)$, and $\mathbf{h}_x = \mathbf{h}_t$, by defining $\mathbf{h} \stackrel{\text{def}}{=} \mathbf{f}_x \circ \mathbf{g}_x = \mathbf{f}_t \circ \mathbf{g}_t$, we can rewrite Eq. (10) as:

$$\begin{aligned} 2 \mathbb{E}_{(\mathbf{z}_x, \mathbf{z}_t) \sim p(\mathbf{z}_x, \mathbf{z}_t)} [d(\mathbf{h}(\mathbf{z}_x), \mathbf{h}(\mathbf{z}_t))/\tau] &+ \mathbb{E}_{\mathbf{z}_x \sim p(\mathbf{z}_x)} \left[\log \mathbb{E}_{\mathbf{z}_t \sim p(\mathbf{z}_t)} [e^{-d(\mathbf{h}(\mathbf{z}_x), \mathbf{h}(\mathbf{z}_t))/\tau}] \right] \\ &+ \mathbb{E}_{\mathbf{z}_t \sim p(\mathbf{z}_t)} \left[\log \mathbb{E}_{\mathbf{z}_x \sim p(\mathbf{z}_x)} [e^{-d(\mathbf{h}(\mathbf{z}_x), \mathbf{h}(\mathbf{z}_t))/\tau}] \right]. \end{aligned} \quad (37)$$

We then connect the right-hand side of Eq. (32) with Eq. (37). To this end, since the two terms in the right-hand side of Eq. (32) are symmetrical, we focus on one of the two terms for convenience, e.g.,

$\mathbb{E}_{\mathbf{z}_x \sim p(\mathbf{z}_x)} [H(p(\mathbf{z}_t|\mathbf{z}_x)), q_{\mathbf{h}}(\mathbf{z}_t|\mathbf{z}_x))]$. It can be shown that:

$$\mathbb{E}_{\mathbf{z}_x \sim p(\mathbf{z}_x)} [H(p(\mathbf{z}_t|\mathbf{z}_x)), q_{\mathbf{h}}(\mathbf{z}_t|\mathbf{z}_x))] \quad (38)$$

$$= \mathbb{E}_{\mathbf{z}_x \sim p(\mathbf{z}_x)} \left[\mathbb{E}_{\mathbf{z}_t \sim p(\mathbf{z}_t|\mathbf{z}_x)} [-\log q_{\mathbf{h}}(\mathbf{z}_t|\mathbf{z}_x)] \right] \quad (39)$$

$$= \mathbb{E}_{(\mathbf{z}_x, \mathbf{z}_t) \sim p(\mathbf{z}_x, \mathbf{z}_t)} [\delta(\mathbf{h}(\mathbf{z}_x), \mathbf{h}(\mathbf{z}_t))/\tau + \log C_q(\mathbf{z}_x)] \quad (40)$$

$$= \mathbb{E}_{(\mathbf{z}_x, \mathbf{z}_t) \sim p(\mathbf{z}_x, \mathbf{z}_t)} [\delta(\mathbf{h}(\mathbf{z}_x), \mathbf{h}(\mathbf{z}_t))/\tau] + \mathbb{E}_{(\mathbf{z}_x) \sim p(\mathbf{z}_x)} [\log C_q(\mathbf{z}_x)] \quad (41)$$

$$= \mathbb{E}_{(\mathbf{z}_x, \mathbf{z}_t) \sim p(\mathbf{z}_x, \mathbf{z}_t)} [\delta(\mathbf{h}(\mathbf{z}_x), \mathbf{h}(\mathbf{z}_t))/\tau] + \mathbb{E}_{(\mathbf{z}_x) \sim p(\mathbf{z}_x)} \left[\log \int e^{-\delta(\mathbf{h}(\mathbf{z}_x), \mathbf{h}(\mathbf{z}_t))/\tau} d\mathbf{z}_x \right] \quad (42)$$

Since $p(\mathbf{z}_x) = |\mathcal{Z}|^{-1}$, and $p(\mathbf{z}_t) = |\mathcal{Z}|^{-1}$ by Lemma 4.2, Eq. (42) is equal to:

$$= \mathbb{E}_{(\mathbf{z}_x, \mathbf{z}_t) \sim p(\mathbf{z}_x, \mathbf{z}_t)} [\delta(\mathbf{h}(\mathbf{z}_x), \mathbf{h}(\mathbf{z}_t))/\tau] + \mathbb{E}_{\mathbf{z}_x \sim p(\mathbf{z}_x)} \left[\log \mathbb{E}_{\mathbf{z}_t \sim p(\mathbf{z}_t)} [e^{-\delta(\mathbf{h}(\mathbf{z}_x), \mathbf{h}(\mathbf{z}_t))/\tau}] \right] + \log |\mathcal{Z}_c| \quad (43)$$

Similarly, for the second term in the right-hand side of Eq. (32), we can proof that:

$$\mathbb{E}_{(\mathbf{z}_t) \sim p(\mathbf{z}_t)} [H(p(\mathbf{z}_x|\mathbf{z}_t)), q_{\mathbf{h}}(\mathbf{z}_x|\mathbf{z}_t))] = \mathbb{E}_{(\mathbf{z}_x, \mathbf{z}_t) \sim p(\mathbf{z}_x, \mathbf{z}_t)} [\delta(\mathbf{h}(\mathbf{z}_x), \mathbf{h}(\mathbf{z}_t))/\tau] \quad (44)$$

$$+ \mathbb{E}_{\mathbf{z}_t \sim p(\mathbf{z}_t)} \left[\log \mathbb{E}_{\mathbf{z}_x \sim p(\mathbf{z}_x)} [e^{-\delta(\mathbf{h}(\mathbf{z}_x), \mathbf{h}(\mathbf{z}_t))/\tau}] \right] + \log |\mathcal{Z}_c|. \quad (45)$$

By combining Eq. (43) and Eq. (45), we can conclude the proof.

E.2 Identifiability result on Convex Bodies

Theorem 4.3 represents a symmetrical adaptation of Theorem 3 from [67]. This alignment allows us to employ Propositions 4, Lemma 1 and Lemma A from [67] to demonstrate that the global minimization of the objective outlined in Eq. (32), as specified in Theorem 4.3, identifies the latent variables \mathbf{z}_x , as well as \mathbf{z}_t , up to linear transformations. For completeness, a brief proof is provided herein, with comprehensive details available in the original work. Clearly, the global minimum of the cross-entropy between two distributions is reached if they match by value and have the same support. Therefore, for the optimal solution of the objective loss Eq. (10) in Theorem 4.3, we have:

$$p(\mathbf{z}_t|\mathbf{z}_x) = q_{\mathbf{h}}(\mathbf{z}_t|\mathbf{z}_x), \quad (46)$$

This expression also holds true for $\mathbf{z}_t = \mathbf{z}_x$, we have:

$$\begin{aligned} C_p(\mathbf{z}_x)^{-1} e^{-\delta(\mathbf{z}_x, \mathbf{z}_x)/\lambda} &= C_q(\mathbf{z}_x)^{-1} e^{-\delta(\mathbf{h}(\mathbf{z}_x), \mathbf{h}(\mathbf{z}_x))/\tau}, \\ \Leftrightarrow C_p(\mathbf{z}_x) &= C_q(\mathbf{z}_x) \end{aligned} \quad (47)$$

As the normalization constants are identical we get for all $\mathbf{z}_x, \mathbf{z}_t$,

$$\delta(\mathbf{z}_x, \mathbf{z}_t) = \lambda \delta(\mathbf{h}(\mathbf{z}_x), \mathbf{h}(\mathbf{z}_t))/\tau. \quad (48)$$

Then, by limiting δ be an L^α metric for $\alpha \geq 1$, $\alpha \neq 2$ or the α -th power of such an L^α metric, using the Theorem 5 in [67], Theorem 4.3 can identify the latent variables \mathbf{z}_x and \mathbf{z}_t up to a permutation transformation, *i.e.*, the recovered latent variable $\mathbf{f}_x(\mathbf{x})$, obtained through the minimization of Eq. (8), is related to the true \mathbf{z}_x as follows: $\mathbf{f}_x(\mathbf{x}) = \mathbf{P}\mathbf{z}_x + \mathbf{c}$, where \mathbf{P} represents a permutation matrix with scaling, and \mathbf{c} is a constant vector.

F Differences from Previous Analysis for Multimodal Contrastive Learning

This work differs from previous works focusing on identifiability analysis for multimodal settings [8, 62, 14] across the following three key dimensions.

Modeling Setting This work proposes modeling transferable knowledge across modalities by latent coupled variables. In contrast, previous works [8, 62, 14] often achieve this by introducing the same/shared variables. The advantages of employing latent coupled variables are thoroughly justified in Section 2. Loosely speaking, From the perspective of model flexibility, the proposed model can be considered a generalization of previous works. This generalization is apparent as the proposed model seamlessly reduces to a single-modal setting when the mixing functions from latent space to observed space are enforced to be identical, and specific variables are omitted.

Identifiability Results The identifiability results obtained in this work diverge from those found in previous works [8, 62], both in terms of breadth and depth of identifiability, due to the introduction of the undirected edge between \mathbf{z}_x and \mathbf{z}_t . a) *Breadth of Identifiability*: Unlike earlier works that often achieve only partial identifiability of latent coupled variables \mathbf{z}_x or \mathbf{z}_t , *e.g.*, latent content variables but not latent style variables [8, 62], our model extends this scope to ensure complete identifiability of latent coupled variables \mathbf{z}_x and \mathbf{z}_t . b) *Depth of Identifiability*: In terms of depth, this work identifies latent coupled variables \mathbf{z}_x and \mathbf{z}_t up to linear or permutation transformations. As a result, after applying a linear ICA method, we can obtain component-wise identifiability, *i.e.*, recovering independent latent variables up to permutation and scaling. This level of precision offers an enhancement over the block identifiability result in previous studies [8, 62], which only identifying latent variables up to a nonlinear invertible mapping, even for independent latent variables. *The differences above in both breadth and depth of identifiability results enable us, for the first time, to unveil the component-wise disentanglement capabilities of multimodal contrastive representation learning.*

Practical Significance in Real Applications Prior studies [8, 62, 14] have predominantly relied on simulation experiments, which often encounter a substantial gap between the assumptions made in theoretical analyses and the practical conditions of real-world applications. In contrast, our work bridges this gap by validating our theoretical findings using pre-trained CLIP models on over 16 diverse real-world datasets. This empirical approach not only substantiates the practical effectiveness of our theoretical results but also demonstrates their applicability and robustness in real-world multimodal settings, highlighting a significant departure from previous work in terms of real-world applicability.

G Differences from Previous Analyses for Single-Modal Contrastive Learning

This work sets itself apart from prior studies focused on the analysis of single-modal contrastive learning [67, 58] in the following key aspects.

Problem Context Previous works primarily address single-modal scenarios, whereas our proposed model extends this framework to the more complex multimodal domain. This extension can be viewed as a generalization of prior approaches. Specifically, our model naturally reduces to a single-modal setting when the mixing functions from the latent space to the observed space are identical, and certain variables are omitted. By expanding the scope to multimodal data, our approach addresses the limitations of prior studies and provides a more comprehensive understanding of contrastive learning.

Technical Perspective Addressing multimodal settings requires significantly broader technical developments compared to single-modal analyses. To this end, we developed Theorem 3.1, which generalizes the asymptotic analysis of contrastive learning to the multimodal context, providing a robust theoretical foundation. Bridging the gap between single-modal and multimodal settings also necessitated novel theoretical insights. For instance, Theorem 4.1 and Theorem 4.3 establish critical connections between multimodal contrastive learning and traditional single-modal frameworks, enabling a unified understanding across these domains. These results not only expand the applicability of contrastive learning but also highlight the intricate dependencies introduced by multimodal data.

New Insights In the multimodal context, a key challenge is effectively modeling the connections between different modalities. This motivates the central insight of our work: latent coupled variables, linked by a unidirectional edge, provide a foundation for exploring whether partial causal models are sufficient for multimodal learning. As highlighted in the introduction, we offer theoretical support for the success of multimodal contrastive learning, including guarantees for its disentanglement capabilities. From a practical perspective, we recommend refining representations from pre-trained CLIP-like models rather than using them directly. Specifically, applying linear ICA methods, such as FastICA (aligned with assumptions on the hypersphere), or combining PCA and FastICA (aligned with assumptions on convex bodies), can enhance

performance on tasks that rely on disentangled representations. These insights not only validate the robustness of our theoretical findings but also emphasize their practical significance in real-world applications.

H More Results on CelebA

Figures 6 - 8 illustrate the 16 distinct disentangled representations obtained using pre-trained CLIP with FastICA. Interestingly, our method achieves competitive results compared to specialized disentanglement techniques, such as FactorVAE [33] and β -TCVAE [6]. Specifically, FactorVAE identified 8 disentangled attributes, while β -TCVAE reported 15, whereas our approach successfully discerns 16 distinct disentangled representations.

It is important to note that this comparison is not meant to position our method as a more effective disentanglement technique. Rather, our experiments are designed solely to validate our theoretical findings. We present this comparison to provide insight into the potential of leveraging CLIP for learning disentangled representations, thereby motivating future research in this direction. A particularly interesting avenue could be exploring how disentanglement capabilities relate to the manipulation of pre-trained vision models, such as diffusion models.

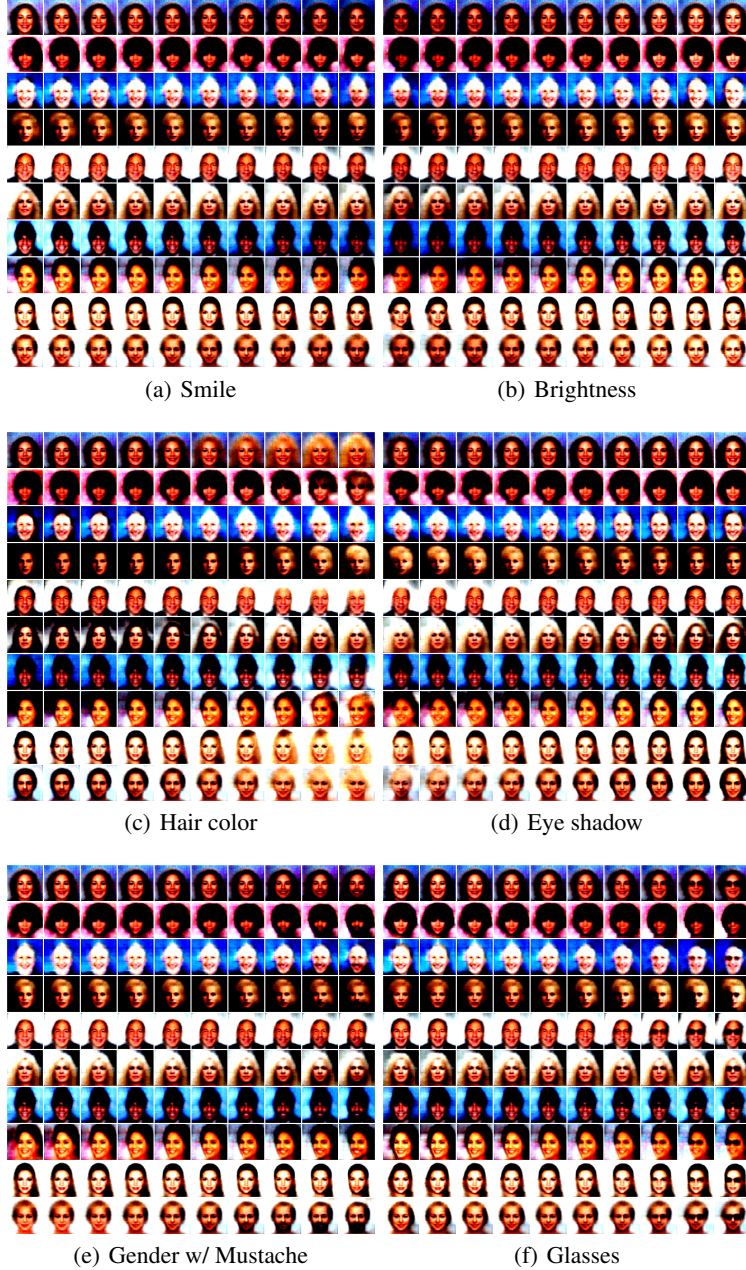


Figure 6: Disentangled Representations learned by combining pre-train CLIP and FastICA.



Figure 7: Disentangled Representations learned by combining pre-train CLIP and FastICA.



Figure 8: Disentangled Representations learned by combining pre-train CLIP and FastICA.

I More Results on ImageNet-Type Data

Table 4: Quantitative results for 16-shot transfer learning and domain generalization by different methods. Lin. P. (Linear Probe).

ENCODERS	METHODS	SOURCE		TARGET (IMAGENET-)			
		IMAGENET	V2	SKETCH	R	A	AVG.
RN50	LIN. P.	55.36	45.45	18.22	34.09	12.52	27.77
	LIN. P. w/ FASTICA	57.82	47.78	19.77	38.05	13.15	29.69
	LIN. P. w/ PCA AND FASTICA	57.37	47.67	20.39	38.76	12.89	29.93
RN101	LIN. P.	60.98	50.36	25.80	46.61	18.64	35.35
	LIN. P. w/ FASTICA	61.86	51.85	27.29	49.29	19.89	37.08
	LIN. P. w/ PCA AND FASTICA	61.58	51.44	28.86	50.32	19.97	37.64
ViT32	LIN. P.	60.76	50.92	28.81	49.18	19.72	37.15
	LIN. P. w/ FASTICA	61.94	51.95	30.30	51.82	20.81	38.72
	LIN. P. w/ PCA AND FASTICA	62.00	52.39	30.39	51.61	20.96	38.84
ViT16	LIN. P.	67.17	57.01	35.43	60.96	35.41	47.20
	LIN. P. w/ PCA AND FASTICA	68.12	58.45	38.41	63.89	37.17	49.48
	LIN. P. w/ FASTICA	67.96	58.38	38.75	65.45	38.28	50.22

Table 5: Quantitative results for 8-shot transfer learning and domain generalization by different methods. Lin. P. (Linear Probe).

ENCODERS	METHODS	SOURCE		TARGET (IMAGENET-)			
		IMAGENET	V2	SKETCH	R	A	AVG.
RN50	LIN. P.	49.33	40.83	15.06	31.23	10.99	24.53
	LIN. P. w/ FASTICA	51.99	43.58	15.47	34.35	12.85	26.56
	LIN. P. w/ PCA AND FASTICA	51.42	42.93	17.28	35.53	12.33	27.02
RN101	LIN. P.	55.41	46.04	23.38	43.26	16.88	32.39
	LIN. P. w/ FASTICA	56.59	47.47	22.09	44.59	18.39	33.14
	LIN. P. w/ PCA AND FASTICA	55.84	46.59	23.68	44.94	18.25	33.37
ViT32	LIN. P.	55.17	46.11	25.53	45.32	18.35	33.83
	LIN. P. w/ FASTICA	56.90	47.96	27.62	49.13	20.31	36.26
	LIN. P. w/ PCA AND FASTICA	55.83	46.55	26.54	46.77	18.80	34.67
ViT16	LIN. P.	61.82	52.34	32.26	55.93	32.63	43.29
	LIN. P. w/ FASTICA	63.55	54.81	34.21	61.54	38.21	47.29
	LIN. P. w/ PCA AND FASTICA	63.47	54.32	35.83	61.88	37.35	47.36

Table 6: Quantitative results for 4-shot transfer learning and domain generalization by different methods. Lin. P. (Linear Probe).

ENCODERS	METHODS	SOURCE		TARGET (IMAGENET-)			
		IMAGENET	V2	SKETCH	R	A	AVG.
RN50	LIN. P.	41.34	33.67	11.55	26.27	9.67	20.29
	LIN. P. w/ FASTICA	44.10	36.07	12.75	30.15	11.64	22.65
	LIN. P. w/ PCA AND FASTICA	42.86	35.38	12.29	28.81	9.79	21.57
RN101	LIN. P.	48.23	39.53	18.80	38.10	14.32	27.69
	LIN. P. w/ FASTICA	49.43	41.02	17.49	39.33	15.25	28.27
	LIN. P. w/ PCA AND FASTICA	49.01	40.25	19.26	39.71	14.75	28.49
ViT32	LIN. P.	47.82	39.53	21.51	40.94	15.99	29.49
	LIN. P. w/ FASTICA	49.43	40.66	22.66	41.78	16.41	30.38
	LIN. P. w/ PCA AND FASTICA	49.48	41.09	23.72	43.48	16.77	31.27
ViT16	LIN. P.	54.30	46.06	27.58	50.76	29.24	38.41
	LIN. P. w/ FASTICA	56.65	48.18	28.27	55.50	33.39	41.33
	LIN. P. w/ PCA AND FASTICA	56.16	47.46	30.21	55.49	31.71	41.22

Table 7: Quantitative results for 1-shot transfer learning and domain generalization by different methods. Lin. P. (Linear Probe).

ENCODERS	METHODS	SOURCE		TARGET (IMAGENET-)			
		IMAGENET	V2	SKETCH	R	A	AVG.
RN50	LIN. P.	21.74	18.24	5.68	15.41	6.55	11.47
	LIN. P. w/ FASTICA	23.22	19.68	6.37	13.84	7.21	11.77
	LIN. P. w/ PCA AND FASTICA	24.06	20.26	6.85	17.54	8.05	13.18
RN101	LIN. P.	26.05	21.48	9.90	23.85	10.17	16.35
	LIN. P. w/ FASTICA	27.50	23.33	8.35	17.87	10.71	15.07
	LIN. P. w/ PCA AND FASTICA	28.50	24.17	11.63	26.38	12.28	18.62
ViT32	LIN. P.	26.99	22.99	11.93	25.25	11.56	17.93
	LIN. P. w/ FASTICA	29.21	24.80	9.97	21.23	12.23	17.06
	LIN. P. w/ PCA AND FASTICA	29.05	24.45	12.39	27.61	12.56	19.25
ViT16	LIN. P.	32.42	27.64	16.34	34.28	21.84	25.02
	LIN. P. w/ FASTICA	34.35	29.31	13.91	28.61	23.24	23.77
	LIN. P. w/ PCA AND FASTICA	35.20	30.26	19.17	38.87	26.41	28.68

J More Results on Few-Shot Learning Task

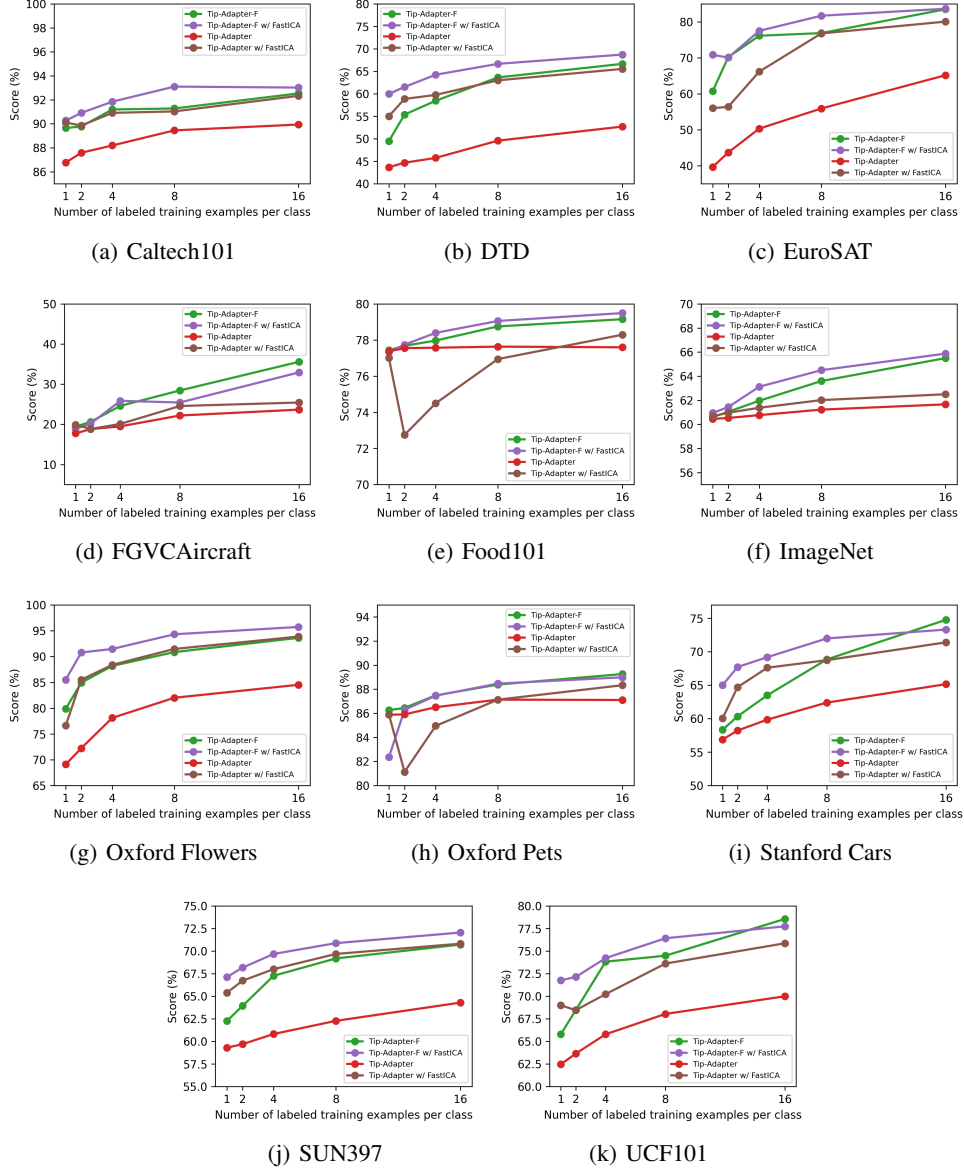


Figure 9: More results on few-shot learning task: A comparison of top-1 accuracy (%) achieved by various few-shot CLIP adaptation methods across 11 datasets. The x-axis indicates the number of training examples per class. The incorporation of FastICA notably enhances the performance of the original methods, Tip-Adapter and Tip-Adapter-F, proposed by [63].

K Implementation Details

We perform all experiments using the GPU RTX 4090, equipped with 32 GB of memory.

Synthetic Data We consider latent coupled variables \mathbf{z}_x and \mathbf{z}_t , each with a dimensionality of 10. Additionally, we have modality-specific latent variables \mathbf{m}_x and \mathbf{m}_t , both set to a dimension of 5. The process begins with sampling from the marginal distribution $p(\mathbf{z}_x)$, and the samples of modality-specific latent variables \mathbf{m}_x and \mathbf{m}_t are obtained by sampling from Gaussian distributions with zero mean and one variance. We then create real pairs by sampling from the conditional distribution $p(\mathbf{z}_t|\mathbf{z}_x)$. The observational data \mathbf{x} and \mathbf{t} are generated using two different Multi-Layer Perceptrons (MLPs). Specifically, we utilize MLPs comprising three hidden layers with leaky ReLU units and random weights. To ensure the invertibility of the MLP g , we carefully control the condition number of the weight matrices. For our encoders concerning both \mathbf{z}_t and \mathbf{z}_x , we adopt an MLP architecture with leaky ReLU units.

Evaluation: To evaluate the linear identifiability result established in Corollary 4.2, we assess how well the learned representations $\hat{\mathbf{z}}_x$ preserve the structure of the ground-truth latent variables \mathbf{z}_x up to a linear transformation. Specifically, we perform the following steps:

1. **Learned Representations Extraction:** We first obtain representations $\hat{\mathbf{z}}_x$ learned by multimodal contrastive learning.
2. **Linear Regression Fitting:** We fit a linear regression model of the form:

$$\hat{\mathbf{z}}_x = \hat{\mathbf{A}}\mathbf{z}_x + \hat{\mathbf{c}} + \epsilon,$$

where $\hat{\mathbf{A}}$ is a learned transformation matrix, $\hat{\mathbf{c}}$ is an offset vector, and ϵ represents residual errors.

3. **Coefficient of Determination (R^2) Computation:** We compute the R^2 score, defined as:

$$R^2 = 1 - \frac{\sum_i \|\hat{\mathbf{z}}_{x,i} - (\hat{\mathbf{A}}\mathbf{z}_{x,i} + \hat{\mathbf{c}})\|^2}{\sum_i \|\hat{\mathbf{z}}_{x,i} - \bar{\hat{\mathbf{z}}}_x\|^2},$$

where $\bar{\hat{\mathbf{z}}}_x$ is the mean of $\hat{\mathbf{z}}_x$. This metric quantifies how well the learned representations can be linearly mapped to the true latent variables.

4. **Analysis Under Different Assumption Violations:** We repeat the evaluation under settings that both satisfy and violate the theoretical assumptions, as listed in Table 1, allowing us to empirically assess the robustness of the identifiability results.

By reporting the R^2 scores across different conditions, we quantify the extent to which multimodal contrastive learning successfully recovers the latent variables up to a linear transformation.

to evaluate permutation identifiability result in Corollary 4.4, we employ the mean correlation coefficient (MCC) between the ground-truth \mathbf{z}_x and representations $\mathbf{f}_x(\mathbf{x})$ learned by multimodal contrastive learning. To compute MCC, we follow these steps:

1. **Compute Correlation Coefficients:** We first calculate the correlation coefficients between all pairs of ground-truth source variables and representations learned by multimodal contrastive learning. Specifically, for each pair of source component $\mathbf{z}_{x,i}$ and recovered latent component $\hat{\mathbf{z}}_{x,j}$, we compute the Pearson correlation coefficient:

$$\rho_{i,j} = \frac{\text{Cov}(\mathbf{z}_{x,i}, \hat{\mathbf{z}}_{x,j})}{\sigma_{\mathbf{z}_{x,i}} \sigma_{\hat{\mathbf{z}}_{x,j}}}, \quad (49)$$

where $\text{Cov}(\cdot, \cdot)$ denotes the covariance, and $\sigma_{\mathbf{z}_{x,i}}$ and $\sigma_{\hat{\mathbf{z}}_{x,j}}$ are the standard deviations of the respective components.

2. **Solve the Linear Sum Assignment Problem:** Since the estimated components may be permuted relative to the ground-truth variables, we solve a linear sum assignment problem to determine the optimal one-to-one mapping between the ground-truth and the learned representations. The goal is to maximize the total absolute correlation across all assigned pairs.
3. **Compute the Mean Correlation Coefficient (MCC):** Given the optimal assignment of the ground-truth variables to the learned representations, we compute the mean of the absolute values of the assigned correlation coefficients:

$$\text{MCC} = \frac{1}{d} \sum_{i=1}^d |\rho_{i,\pi(i)}|, \quad (50)$$

where $\pi(i)$ denotes the index of the assigned representation corresponding to the i th latent variable, and d is the number of latent variables.

A high MCC indicates that the learned representation closely match the true source variables, up to permutation transformations, thereby validating the identifiability of the learned representations.

ReLU(BN(ConvTranspose2d(512, 512, kernelsize=1, stride=1, padding=0)))
ReLU(BN(ConvTranspose2d(512, 64, kernelsize=4, stride=1, padding=0)))
ReLU(BN(ConvTranspose2d(64, 64, kernelsize=4, stride=1, padding=0)))
ReLU(BN(ConvTranspose2d(64, 32, kernelsize=4, stride=1, padding=0)))
ReLU(BN(ConvTranspose2d(32, 32, kernelsize=4, stride=1, padding=0)))
ConvTranspose2d(32, 3, kernelsize=4, stride=2, padding=1)

Table 8: Decoder for the image data.

Disentangled Representation Learning on CelebA To obtain disentangled representations for the CelebA dataset, we initially employ the FastICA implementation available in the scikit-learn software on the representations extracted from the pretrained ViT-B/32 encoder. Subsequently, we train the decoder, as outlined in Table 8, utilizing Mean Squared Error (MSE) loss.

Experiments of Linear Probe In our experiments with ImageNet-Type data, we utilized the PCA and FastICA implementations provided by scikit-learn. For our proposed method, which combines PCA and ICA, we configured the number of components to 500 for PCA, and for FastICA, we set it to 160 for 1, 2, and 4-shot learning scenarios, and 200 for 8 and 16-shot learning scenarios. When employing ICA alone, we chose to use 300 components. For the proposed method with ICA only, we set number of components to 300. Following the setting of linear probe in CLIP, we train a logistic regression classifier using scikit-learn’s L-BFGS implementation, with maximum 1,000 iterations. We determine the L2 regularization strength using a hyperparameter sweep on the validation sets over the range between 10^{-6} and 10^6 , with 96 logarithmically spaced steps. To save compute required for the sweeps, we perform a parametric binary search and iteratively halves the interval around the peak until it reaches a resolution of 8 steps per decade. The hyperparameter sweeps are performed on a validation split of each dataset.

FastICA as a plug-and-play Tool. We incorporate FastICA in the framework proposed in [63] to enhance its ability for few shot learning. The framework consists of two primary modules: one keeps the zero-shot capabilities of pre-trained CLIP, ensuring effective utilization of prior knowledge, while the other, the cache module, constitutes the central contribution of the work. The cache module endeavors to transfer knowledge from labeled training samples. Given the above, we integrate FastICA into the cache module, preserving the invaluable prior knowledge derived from the zero-shot abilities of pre-trained CLIP. For parameter settings in FastICA, we opted for 100 components for the majority of datasets. Specifically, we assigned 350 components for the ImageNet dataset, 300 components for the OxfordPets dataset, and 50 components for the EuroSAT dataset. A learning rate of 0.1 was employed for implementation. For the remaining parameter settings, we adhered to the specifications outlined by [63].